Flow (2023), **1** E1
doi:10.1017/flo.2023.1

FLOW CAMBRIDGE UNIVERSITY PRESS

RESEARCH ARTICLE

A Review and Reassessment of the Aerodynamics of Cricket Ball Swing

Sam D. Grimshaw*, Aaron Briggs and Nick R. Atkins

Whittle Laboratory, Department of Engineering, University of Cambridge
*Corresponding author. E-mail: sdg33@cam.ac.uk

Received: 1 December 2023; **Revised:** 1 February 2024; **Accepted:** TBC

Keywords: Boundary Layer Aerodynamics; Cricket Ball Swing; Sports Aerodynamics

Abstract

This paper reviews 70 years of cricket ball swing literature and reassesses the results in light of new measurements. A comparison of ball tracking data with published experimental results shows that current understanding does not explain the behaviour observed in professional cricket matches. Descriptions of cricket ball boundary layer aerodynamics are updated with new results which show that the seam acts more like a series of vortex generators than a trip and that there is a laminar separation bubble on the seam side of the ball. Previous results for reverse swing are consolidated and compared to new data, showing that different magnitudes of swing occur depending on the condition of both sides of the ball. Variation in pressure and temperature should be included when Reynolds number, a non-dimensional ball speed, is calculated, while humidity can be neglected. Studies on the effect of wind speed and direction are summarised and results considering the effect of freestream turbulence are compared with new measurements. Throughout the paper, recommendations for future work are suggested. These include quantitative study of the effect of surface defects and roughness, an assessment of whether atmospheric turbulence can affect swing, and investigation into the effect of backspin on swing.

Impact Statement

The phenomenon of cricket ball swing is reviewed and reassessed using new results recorded for this paper. Swing bowling impacts the outcome of cricket matches, however, the existing scientific literature does not fully capture the behaviour recorded by ball tracking data in professional matches. This means that personal experience and anecdote still drive players, coaches, pundits and fans' thinking around swing. Better understanding of the phenomenon will improve talent identification, coaching, selection, tactics and the wider public's enjoyment of the game.

The boundary layer aerodynamics responsible for swing are systematically described for varying Reynolds number, ball surface condition and freestream turbulence to provide a comprehensive description of the physical mechanisms at play. Existing explanations are predominantly qualitative in nature, however, and the paper identifies further work needed to quantify realistic boundary conditions and their effect, and to analyse the problem within a statistical framework.

1. Introduction

The sport of cricket is a contest between two teams who are striving to score as many runs as possible. Each team takes turn to bowl at the opposition batters who attempt to hit the cricket ball and score runs. If a batter makes a mistake they may lose their wicket, meaning that their role in the innings is over and

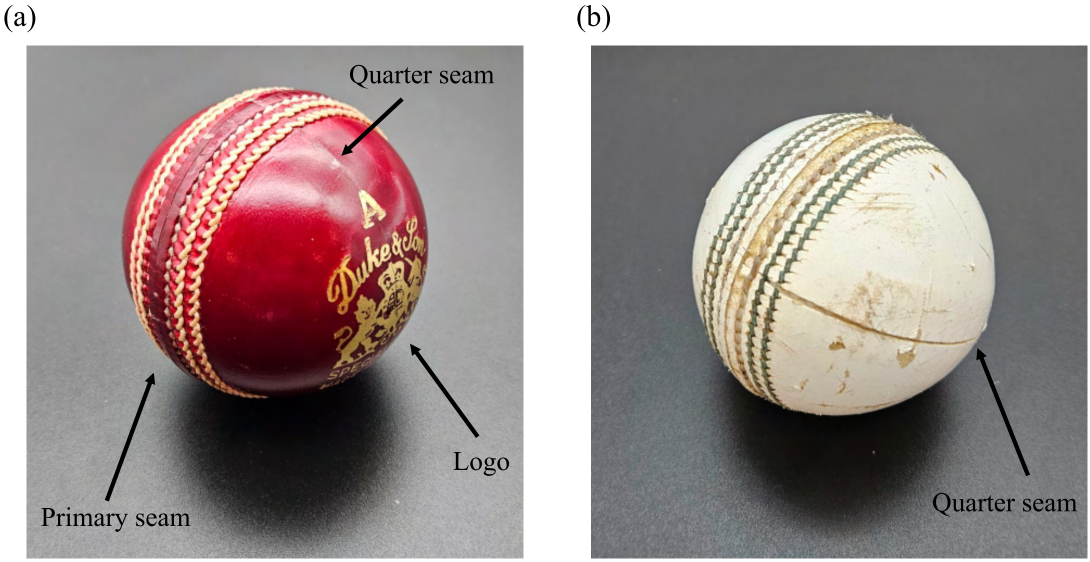

Figure 1. *(a) New red ball used in Test Matches; (b) Worn white ball used in a One Day International Match.*

a new batter has to try their luck. While the sport contains many laws and intricacies, it is the battle between bat and ball that has made cricket one of the world's most popular sports, with over 1 billion fans and 300 million participants worldwide [1].

'Swing' bowling is a technique used by 'fast bowlers', who deliver the ball at speeds ranging from 60 to 100 miles per hour (27 to 45m/s). A ball is said to swing when its trajectory curves after the ball is released and before it bounces. A batter's reaction time in professional cricket is less than 0.5s [2] and swing makes it more difficult to judge a ball's flightpath, reducing the number of runs scored and increasing the chance of wickets being taken [3].

Cricket balls are made from a cork core wrapped in string with a leather casing. A raised, 'primary' seam runs around the middle of the ball and perpendicular to this are two tightly stitched 'quarter seams'. At the start of an innings the ball is in pristine condition with a shiny, lacquered surface and undamaged seams. Figure 1(a) shows a new red ball used in Test Cricket matches in England. As a cricket match progresses the ball wears as it hits the bat and the ground. The leather becomes rough, the raised seam can be damaged or compressed, and the quarter seams can begin to split. A worn, white cricket ball used in a One Day International match is shown in Fig. 1(b).

1.1. Overview of Cricket Ball Swing Literature

Numerous academic papers have been published explaining how the behaviour of the flow immediately adjacent to the ball, called the boundary layer, results in a sideways force which causes the ball to swing. These theories were first presented in the 1950s by Cooke [4] and Lyttleton [5] and in the following years, experiments by Harrington and Southworth [6], Burgess and Probert [7] and Moore and Needes [8] were performed to test the ideas. Horlock's 1973 paper [9] summarises this early work, combining wind tunnel test data with boundary layer theory to explain why cricket balls swing.

Since the 1980s, Mehta has produced three review papers [10, 11, 12], and a similar summary paper was also produced by Verma [13]. These consolidate established ideas and identify topics for further study. Over the last ten years, researchers have continued to investigate cricket ball swing using new techniques including infra-red visualisation of surface flow (Scobie et al. [14]), particle image velocimetry (Jackson et al. [15]) and computational fluid dynamics (Tom et al. [16]) to uncover further details about swing. However, despite undoubted progress, the impact of academic work on professional cricket has been limited as it has been unable to explain or predict swing as it is observed on the field of play. This discrepancy is illustrated in the next subsection, where ball tracking data from cricket matches is compared with published results obtained from wind tunnel tests.

1.2. Comparison of Ball Tracking Data with Wind Tunnel Measurements

Ball tracking technology, which utilises multiple high-speed video cameras and triangulation software, was introduced to cricket in 2001 to provide information about the trajectory of cricket ball deliveries. It is now widely adopted in international and professional cricket where it aids match officials in decision making, provides statistics and insight for television viewers, and is used by teams and players for performance analysis [17].

Section 3 in this article shows how a non-dimensional swing force coefficient, C_S, is calculated from ball trajectory data and Fig. 2 demonstrates how the database can be analysed to study trends in the behaviour of cricket ball swing. C_S is defined in Eq. 1 in Section 2, and provides a measure of the force causing the ball to swing. C_S has a magnitude, $|C_S|$, and direction denoted by its sign, so that increased $|C_S|$ corresponds to more swing. A delivery with $C_S = 0$ corresponds to a straight delivery which does not swing.

Figure 2(a) shows the distribution of $|C_S|$ for 6982 balls delivered in the first 'over' (six legal deliveries) of Test Cricket matches between 2006 and 2018, with a release speed greater than 60mph (27m/s). The direction of swing is not plotted, as the aim is to capture both 'in-swing' and 'out-swing' deliveries. The histogram shows that for new balls, 44% of deliveries have $|C_S|$ less than 0.1, 41% are between 0.1 – 0.3, and 15% are greater than 0.3.

Most previous work on cricket ball swing begins by considering the behaviour of new balls. A compilation of C_S results, from various studies, is presented in Fig. 6 in Section 4. These results are recorded using a ball mounted in a wind tunnel so that C_S can be measured. The results of the different wind tunnel tests are consistent; $|C_S|$ measured is either high, between 0.2 and 0.35 or low, less than 0.1, and the continuous distribution of $|C_S|$ observed on the field and presented in Fig. 2, is not reproduced.

Figure 2(b) shows the distribution of $|C_S|$ for old balls in Test Cricket. This data comprises 99,913 deliveries released at a speed greater than 60mph (27m/s) with a ball aged between 40 and 80 overs old. The histogram shows that the distribution of $|C_S|$ is shifted to lower values compared to the opening over shown in Fig. 2(a): 53% of deliveries have $|C_S|$ less than 0.1, 43% are between 0.1 and 0.3 and 4%

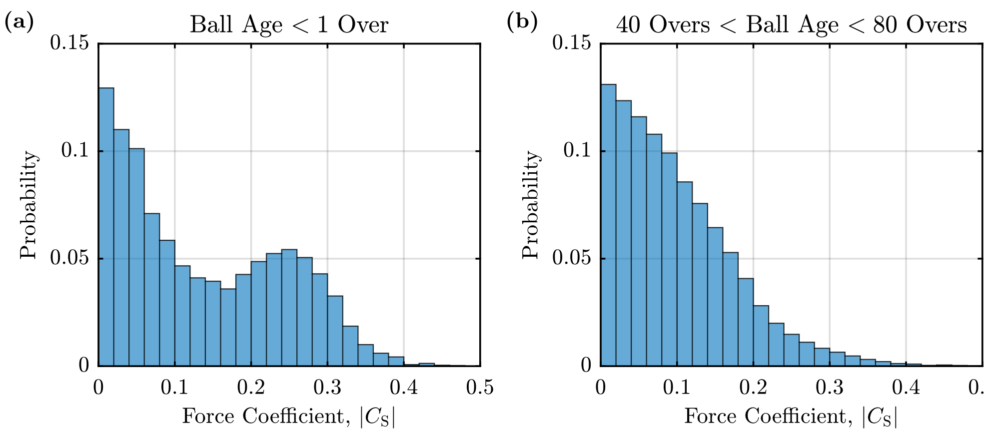

Figure 2. *Distribution of swing force coefficient magnitude, $|C_S|$, in Test Match cricket from 2006 - 2018, calculated from ball tracking data for:* ***a)*** *Ball age less than 1 over* ***b)*** *Ball age between 40 and 80 overs.*

are larger than 0.3. Measurements of old cricket balls presented in the literature are reproduced in Fig. 7 in Section 4. Unlike new balls, this data shows a continuous spread of $|C_S|$ between 0 and 0.35 which agrees qualitatively with the ball tracking data for old balls. Our literature review concludes, however, that the mechanisms which produce this spread of C_S for old balls has not been fully explained and a quantified relationship between ball condition and swing has not been established.

1.3. Paper Aims and Layout

This paper provides an up-to-date review and reassessment of published research on cricket ball swing. It also presents new data, including simultaneous force and infra-red (IR) flow visualisation measurements, obtained from wind tunnel tests performed at the Whittle Laboratory in Cambridge, UK. The paper has two objectives: first, it seeks to confirm previously published explanations for cricket ball swing and update these where necessary. Second, it aims to identify topics for further research which will enable the behaviour observed in cricket matches using ball tracking data, for example in Fig. 2, to be explained and modelled.

The paper is split into five further sections. In Section 2, the nomenclature and terminology of cricket ball swing and boundary layers are defined and in Section 3 the assumptions and methods used to process the ball tracking data shown in Fig. 2 are described. Section 4 reviews papers which discuss how cricket ball boundary layer behaviour causes swing and compares published results with new wind tunnel measurements. Section 5 considers papers which have studied realistic boundary conditions which include the effect of ball rotation and atmospheric conditions, and finally, Section 6 presents conclusions along with recommendations for future work.

2. Nomenclature and Terminology

2.1. Cricket Ball Swing

As the literature around cricket ball swing has grown, a common nomenclature and terminology has developed which is summarised in Fig. 3. Here the ball is viewed from 'top down' and the swing and drag forces, F_S and F_D, act perpendicular and in line with the direction of flight respectively. The seam angle, θ, defines the angle between the seam centre line and direction of flight while the rotation angle, α, and rate, ω, are defined perpendicular to the seam centre line. The side of the ball where the flow passes over the seam at the front of the ball is called the 'seam side' and the other side is called the 'non-seam side'. Separation points are quantified by separation angle, ϕ_s and are measured from the stagnation point at the front of the ball to the point where the boundary layer separates and forms a wake.

In this article, forces are non-dimensionalised by the dynamic pressure acting on the ball as defined in Equation 1:

$$C_S = \frac{F_S}{\frac{1}{2}\rho A U^2} \tag{1}$$

where ρ is air density, A is the frontal area of the ball and U is ball speed. Ball geometry, speed and the properties of air are also combined to evaluate Reynolds number:

$$Re = \frac{\rho U D}{\mu} \tag{2}$$

where D is ball diameter and μ is the dynamic viscosity of air. Re represents the ratio of inertial to viscous forces in a flow and strongly influences boundary layer behaviour, discussed in the next subsection.

There are two types of cricket ball swing: 'conventional swing' and 'reverse swing'. For conventional swing, the swing force acts towards the seam side, and the ball swings in the direction that the seam is

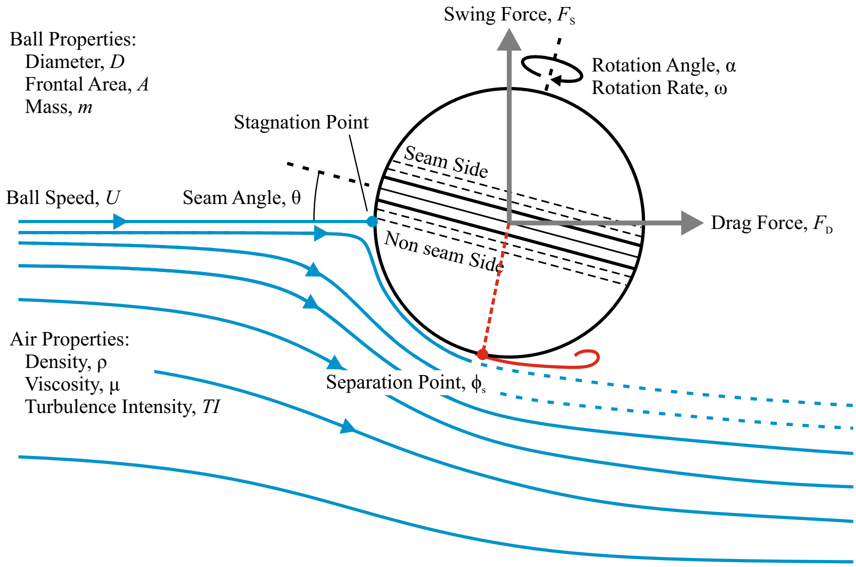

Figure 3. *Top down view of cricket ball including sketch of streamlines passing the non-seam side and variables related to swing.*

pointing, as shown in Fig. 3. Reverse swing acts in the opposite direction; the swing force is towards the non-seam side and the ball swings away from the direction the seam is pointing. In this paper, swing force is defined as positive for conventional swing and negative for reverse swing in line with other studies.

2.2. Boundary Layer Behaviour

Publications on cricket ball swing often discuss boundary layers though there is some inconsistency in the terms used in different papers. This subsection defines the terminology for describing boundary layers based on Schlichting's seminal work on the topic [18].

A boundary layer is the region of flow close to a surface where the flow velocity is slowed by viscous interactions with a 'no-slip condition' at the wall. For a cricket ball in flight, the boundary layer is best described in a frame of reference moving with the ball. The ball then appears stationary, with flow approaching at the flight speed and a no-slip condition at the ball surface. Within the boundary layer the flow can be 'laminar' or 'turbulent' and these different types of boundary layer are illustrated in Fig. 4. Laminar flow is layered, with sheets of fluid moving "*with different velocities without great exchange of fluid particles perpendicular to the flow direction* [18]". Turbulent flow "*is characterised by a highly irregular, random, fluctuating motion* [which is] *superimposed on the regular basic flow and leads to large amounts of mixing perpendicular to the flow direction* [18]". It is the transverse mixing motion which causes momentum exchange normal to the flow direction in turbulent boundary layers.

At low values of Re, flows are laminar but as Re increases above a 'critical' value there is a 'transition' to turbulent flow. Transition occurs at a point when the boundary layer flow becomes unstable and small disturbances are able to grow and propagate, leading to a turbulent boundary layer. Laminar to turbulent transition in boundary layers is affected by a number of factors alongside Re. The most important of these for studying cricket ball swing are the freestream turbulence and surface roughness.

When a boundary layer forms on a curved surface, such as that of a cricket ball, it experiences a pressure gradient in the streamwise direction. An 'adverse pressure gradient' is experienced when the pressure increases in the direction of flow, $\mathrm{d}p/\mathrm{d}s > 0$, and velocity reduces. The deceleration of the

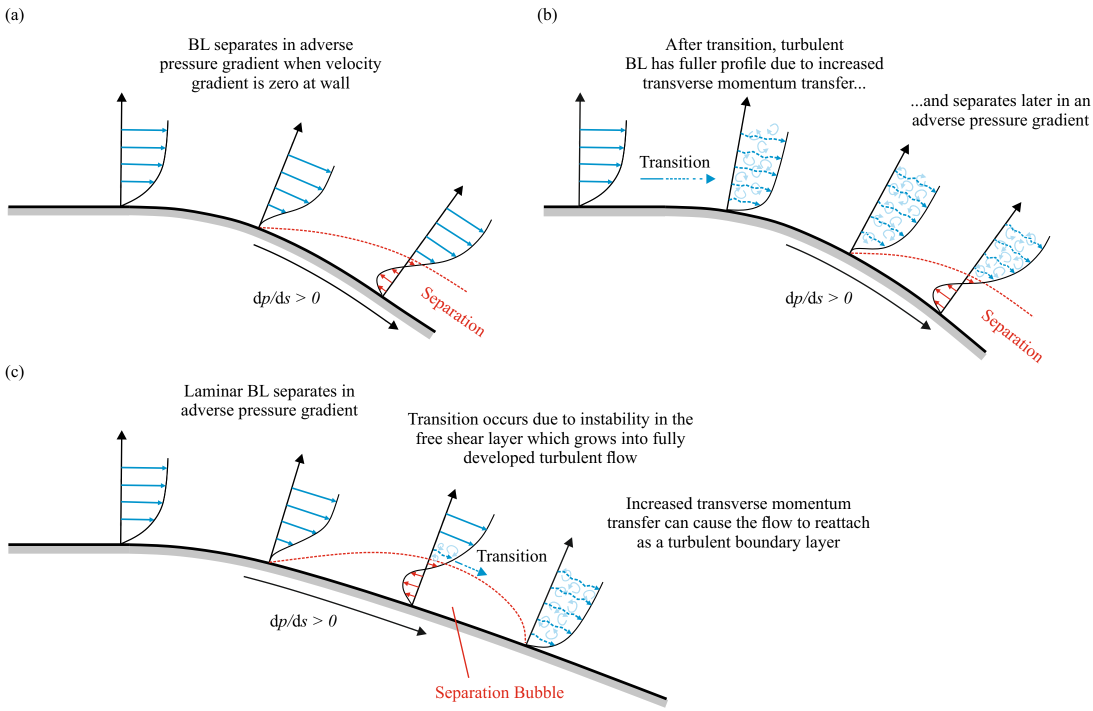

Figure 4. *Illustrations of boundary layer behaviour. Unsteady, turbulent flow is represented by 'eddies' superposed over dashed lines. (a) Laminar boundary separation; (b) Transition and turbulent boundary layer separation; (c) Laminar boundary layer separation and turbulent reattachment.*

boundary layer flow causes it to undergo 'separation' when the velocity profile becomes inflected and the velocity gradient at the wall is zero. Downstream of this point, the flow close to the surface reverses and a separation forms as shown in Fig. 4. For the same adverse pressure gradient, a turbulent boundary layer remains attached for longer than a laminar boundary layer due to the increased transverse momentum transfer associated with turbulent flow. Adverse pressure gradients also promote turbulent transition as their effect on the velocity profile acts to reduce the stability of a laminar boundary layer.

Under the right conditions, transition can occur in the separated free shear layer downstream of a laminar boundary layer separation, as shown in Fig. 4(c). A recent review of this topic is provided by Yang [19] and this explains that for low levels of turbulence intensity, $< 3\%$, transition occurs due to an instability in the shear layer growing into fully developed turbulent flow. In the separated flow, the viscous damping is reduced compared to an attached boundary layer causing the transition to turbulence to occur over a shorter streamwise distance. Once the flow is turbulent, the increase in transverse momentum transfer can cause the flow to 'reattach' to the surface. When this happens the flow between the separation and reattachment becomes trapped and forms a 'separation bubble'.

The boundary layer flows observed around cricket balls are characterised by the behaviours described above and illustrated in Fig. 4. The differences in separation position between laminar, turbulent and reattached turbulent boundary layers is the underlying mechanism for generating a swing force on a cricket ball.

3. Cricket Ball Trajectories and Quantifying Swing using Ball Tracking Data

Since 2001, ball speed and position have been recorded during international cricket matches using high speed cameras and ball tracking software [17]. This section considers the trajectory of a cricket ball delivery and explains how the ball tracking database is processed to provide force coefficient distributions like that shown in Fig. 2.

Swing is caused by an aerodynamic force acting in a horizontal plane, perpendicular to the direction of ball flight. A ball's trajectory can therefore be used to determine the forces acting upon it. Figure 5 shows a ball travelling at an average speed U, under the influence of a perpendicular swing force, F_S. Baker's study on the trajectory of a swinging cricket ball, using time dependent equations of motion [20], shows that the same trajectory is formed when considering either instantaneous or time-averaged values for ball speed and force, provided that the C_S and drag force coefficient, C_D, remain constant for the time of flight, t. The ball tracking database does not provide time accurate positions or velocities between release and bounce, so a constant C_S and average speed are assumed for the entire delivery. Equations 3 and 4 show how this analysis produces a parabolic trajectory for a ball travelling a distance l along its initial trajectory, while swinging a distance, s. Here, m is ball mass equal to 0.156kg and a is the ball acceleration perpendicular to its direction of flight.

$$s = \frac{1}{2}at^2 = \frac{F_S}{2m}t^2 \tag{3}$$

Combining Eq. 3 with Eq. 1 for the non-dimensional swing force coefficient allows the perpendicular displacement, s, to be defined in terms of C_S.

$$s = \frac{\rho A U^2 C_S}{4m}\frac{l^2}{U^2} = \frac{\rho A}{4m}C_S l^2 \tag{4}$$

The relationship between swing force and ball trajectory means that the ball tracking database can be used to calculate an average C_S. C_S can also be measured in wind tunnel experiments and compared directly with values calculated from ball tracking data. Figure 5 shows the parameters recorded: the position of ball release, x_r and y_r, and bounce, x_b and y_b, the ball speed at release, U_r, and when it bounces, U_b, and the 'degree of swing', β_S, which is the change in angle in the $x - y$ plane of the ball trajectory between release and bounce. Noting that $\beta_S < 5°$ gives an expression for s/l:

$$\frac{s}{l} = \tan(\frac{\beta_S}{2}) \approx \frac{\beta_S}{2} \tag{5}$$

Combining Equations 4 and 5 gives an expression for C_S which can be calculated using the values recorded for each delivery in the ball tracking database:

$$C_S = \frac{2m}{\rho A}\frac{\beta_S}{l} \tag{6}$$

The ball mass and frontal area are those specified by the laws of the game and where atmospheric conditions are not recorded, the standard value for air density is used, leading to an error of up to ±10%. Unlike degree of swing, C_S is independent of 'length', the distance between release and bounce, and is also normalised for air density if atmospheric conditions are recorded.

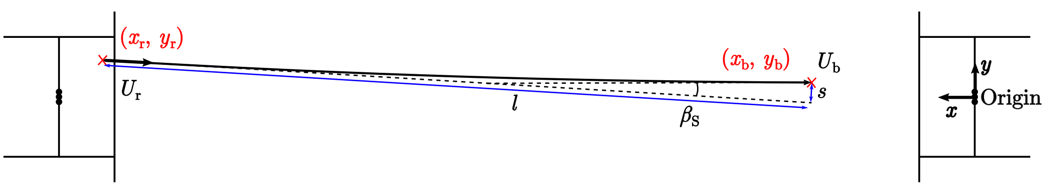

Figure 5. *Top down view of cricket pitch showing ball trajectory and variables recorded by ball tracking.*

4. Boundary Layer Aerodynamics and Cricket Ball Swing

Since the 1970's, researchers have measured swing force using cricket balls mounted on a sting in a wind tunnel. Results showing C_S against Re for new cricket balls, from Scobie et al. [21], Deshpande et al. [22], Sayers and Hill [23] and Alam et al. [24] are reproduced in Fig. 6. Old balls which have been worn through use in a cricket match [14, 21, 25] or aged artificially using sandpaper [22] have also been investigated and results from these experiments are shown in Fig. 7. Included in both figures are measurements performed for this review paper which are labelled 'W'. The experimental methods used to obtain the Whittle Laboratory data are detailed in Appendix A.

The new ball measurements shown in Fig. 6 all exhibit similar behaviour with two regimes observed: when Re is below a specific value for each ball, C_S between 0.25 and 0.35 is recorded, with the positive sign indicating conventional swing. For Re above the specific value, a smaller, negative C_S of between -0.05 and -0.12 is recorded, indicating reverse swing. From a cricketing perspective, $Re = 1.8 \times 10^5$ corresponds to a bowling speed of approximately 85 mph, at standard atmospheric conditions of air density 1.225kg/m^3 and viscosity 1.8×10^{-5}kg/m/s. At this speed, deliveries with $C_S = 0.3$ swing towards the seam side 0.52m if bouncing 15m from release.

For old balls, shown in Fig. 7, there is more variation in the results. Balls A,B,C,E,H,J and K have positive C_S varying between 0.1 and 0.45 for Re below a specific value for each ball. At higher Re these balls display reverse swing with negative values of C_S between -0.1 and -0.3. Balls D,F,G and I, which are older or artificially worn on both sides, have C_S between 0.1 and -0.1 and have undergone the switch from conventional to reverse swing at Re below the range encountered in professional cricket.

Most published work on cricket ball aerodynamics attempts to explain the behaviours observed in Figs 6 and 7 by studying the flow past the non-seam and seam side of the ball and by considering how the changes in boundary layer behaviour cause the ball to swing. This section of our review summarises the literature and compares published results with new data recorded for this paper. Where necessary, physical explanations are refined or updated and previous measurements reassessed based on the new analysis. The discussion is split into five parts: the first subsection covers conventional swing, the second reviews reverse swing, the third considers the switch from conventional to reverse swing, the fourth covers the two-dimensional approximation implicit in most explanations of cricket ball swing, and the fifth provides a summary and lists areas for further study.

4.1. Conventional Swing

Horlock's paper [9], which reports cylinder and cricket ball wind tunnel tests, is the first to show that conventional swing is caused by "*laminar separation on the smooth* [non-seam] *side and turbulent separation on the rough* [seam] *side*". Figure 8(a), reproduced from Mehta [10], confirms the asymmetric nature of the flow with different separation points observed on the non-seam and seam sides using smoke flow visualisation. It should be noted that this test was performed at $Re = 0.85 \times 10^5$, approximately half of that encountered in professional cricket. Similar results, showing separation asymmetry but at higher Re, have been obtained by Deshpande et al. [22] where oil flow visualisation was used on an aluminium model of a cricket ball as shown in Fig. 8(b), Scobie et al. [14], who used IR imaging on a model cricket ball as shown in Fig. 8(c), and Jackson et al. [15] who present a top down view of the flow past a model ball using particle image velocimetry (PIV) as shown in Fig. 8(d). Figure 9, reproduced from Scobie et al. [14], shows pressure measurements around an instrumented model cricket ball at $Re = 0.20 \times 10^5$, 1.47×10^5 and 1.95×10^5, assuming standard atmospheric conditions. These measurements allow the authors to estimate the position of separation points on each side and also demonstrate the asymmetric nature of the flow past the ball.

Research by Achenbach [26, 27] into the flow past spheres is referenced in several cricket ball swing papers [28, 14, 21, 15, 25] and Fig. 10 reproduces Achenbach's results showing separation angle plotted against Reynolds Number for spheres with three levels of roughness. For the smooth sphere, the separation point in the sub-critical regime where $Re < 2 \times 10^5$ is 82°. This increases to around

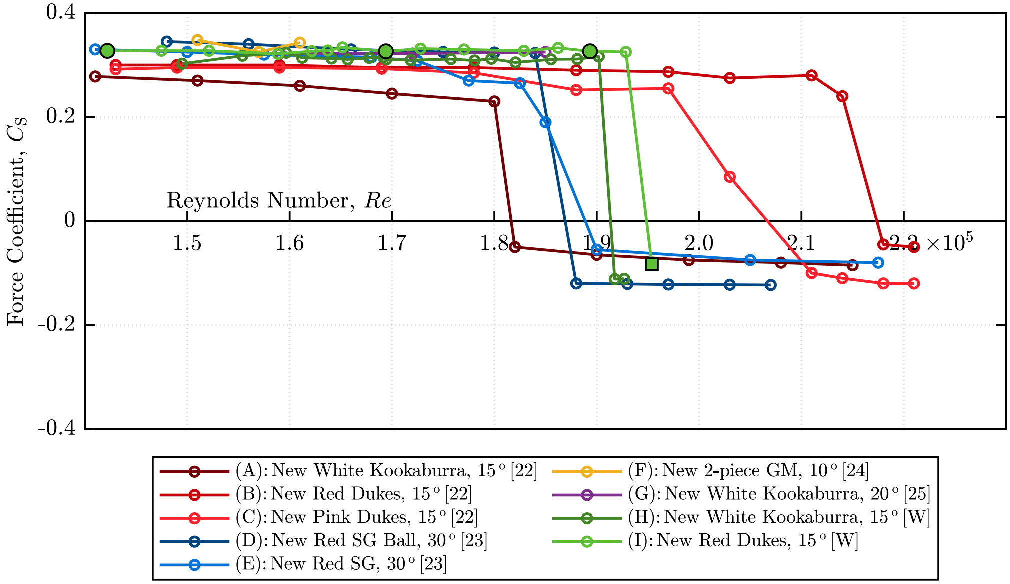

Figure 6. *Swing force coefficient, C_S, for new cricket balls plotted against Reynolds Number, Re, for wind tunnel experiments reported in literature and from Whittle Laboratory tests, labelled 'W'. IR images for conventional swing are presented in Fig. 12 for the three cases highlighted with solid, circular markers. IR images for reverse swing are presented in Fig. 16 for the case highlighted with a solid, square marker.*

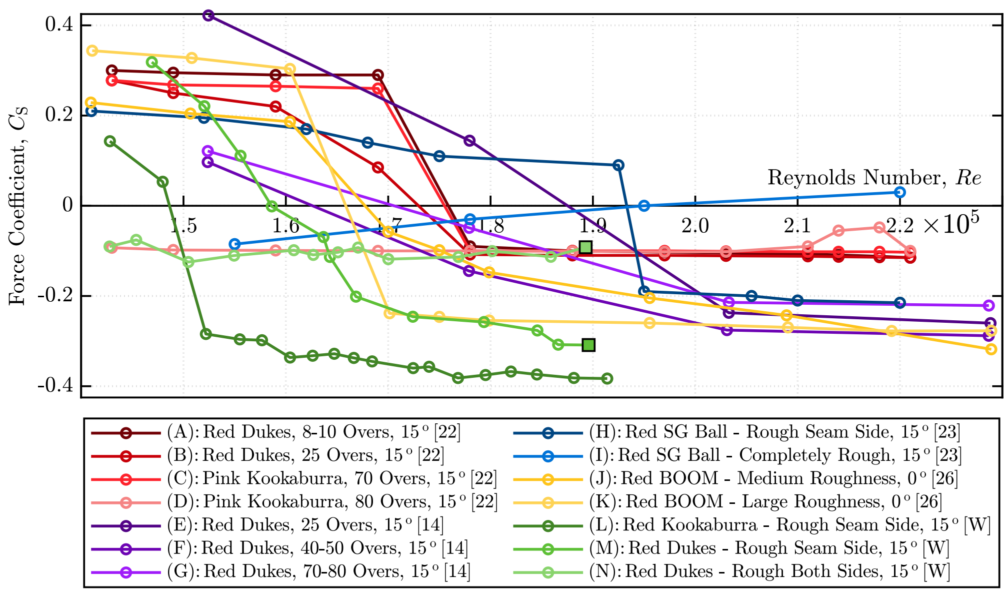

Figure 7. *Swing force coefficient, C_S, for used cricket balls against Reynolds Number, Re, for wind tunnel experiments reported in literature and from Whittle Laboratory tests, labelled 'W'. IR images for reverse swing are presented in Fig. 16 for the two cases highlighted with solid, square markers.*

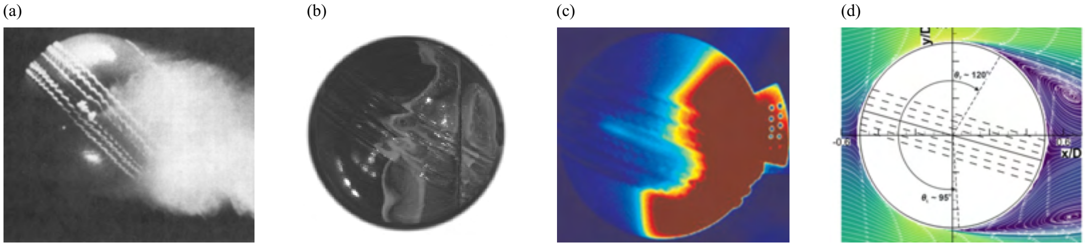

Figure 8. *Flow visualisation experiments from literature illustrating asymmetric separation points for conventional swing. (a) Smoke flow visualisation at Re* = 0.85×10^5 *[10]; (b) Oil flow visualisation on an aluminium model ball at Re* = 2.82×10^5 *[22]; (c) IR imaging of a model cricket ball at Re* = 1.47×10^5 *[14]. Red indicates a separated region where heat transfer from the freestream flow to the ball is low; (d) PIV measurement of model cricket ball at Re* = 1.1×10^5 *[15]. Yellow contours indicate high velocity, dark blue contours indicate zero velocity.*

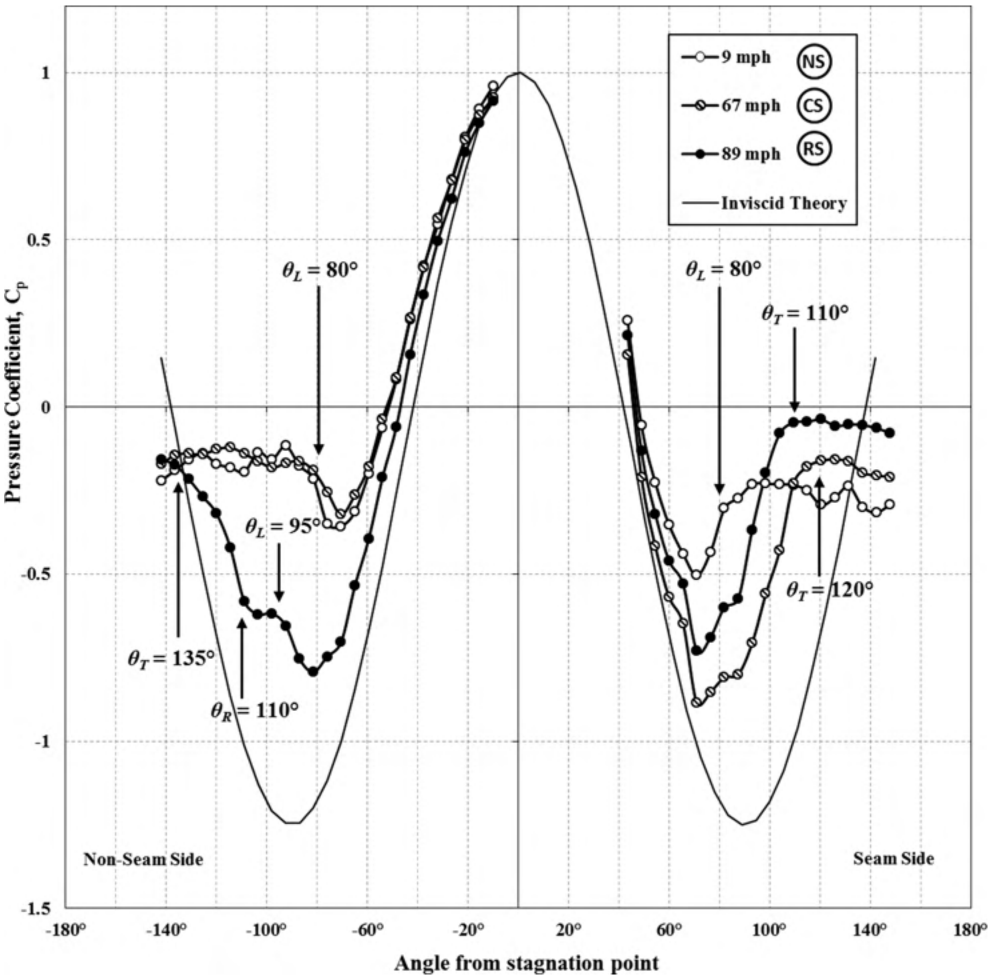

Figure 9. *Variation of pressure coefficient with angle from stagnation point at varying speed [14]. NS: No-swing, CS: Conventional Swing, RS: Reverse Swing. Assuming standard atmospheric conditions, 9mph is equivalent to Re* = 0.20×10^5, *67mph is equivalent to Re* = 1.47×10^5 *and 89mph is equivalent to Re* = 1.95×10^5.

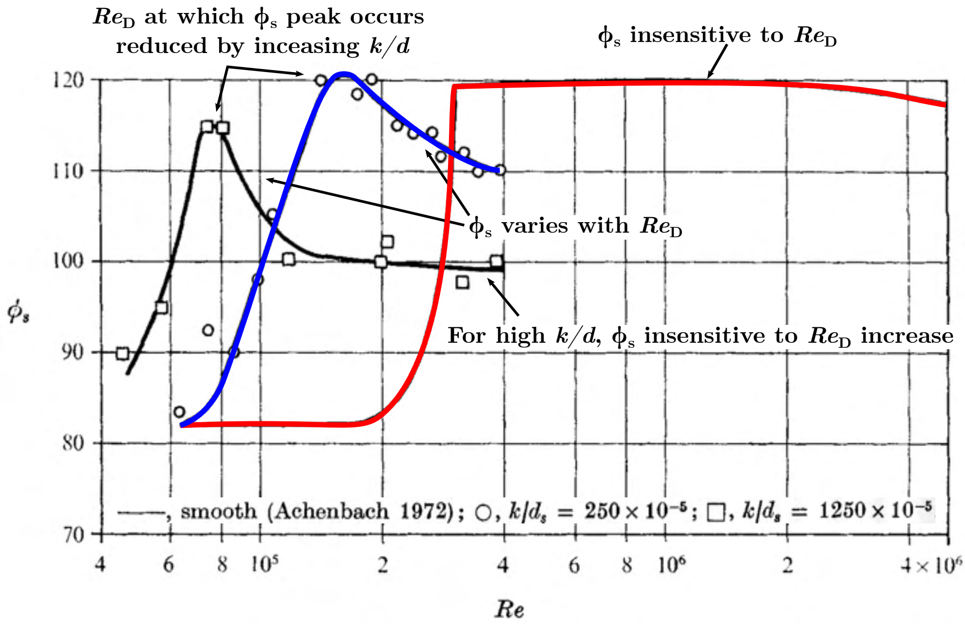

Figure 10. *Variation of separation angle with Reynolds Number for spheres with varying roughness. Reproduced from Achenbach [27].*

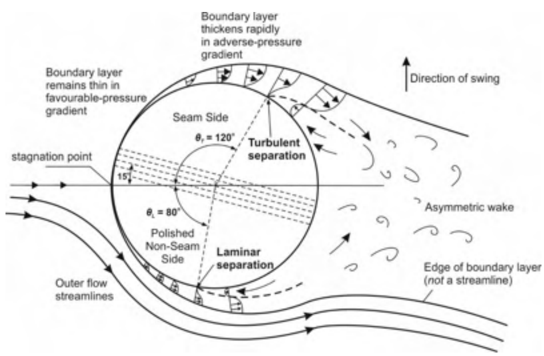

Figure 11. *Top down sketch of flow past a cricket ball for conventional swing. Reproduced from Scobie et al. [21].*

120° in the super-critical regime where $Re > 4 \times 10^5$. Scobie et al. [21] combine their cricket ball measurements with Achenbach's results for spheres, to provide an explanation of conventional swing which is illustrated by the sketch in Fig. 11.

To validate Scobie et al.'s description of conventional swing, infrared images of the non-seam and seam side of a new cricket ball, at Re which result in conventional swing, have been captured at the Whittle Laboratory in Cambridge, UK. A temperature difference between the ball surface and the flow is achieved by chilling the ball to 5°C meaning that areas of low heat transfer appear light, as the surface remains colder than the wind tunnel jet, and regions of high heat transfer appear dark, as the surface is heated by the wind tunnel flow. A description of the experimental methods used to obtain these images is provided in Appendix A. The rest of this subsection on conventional swing is split into an analysis of the flow over the non-seam side, then the seam side, before finally assessing the flow asymmetry.

Non-seam side. Figure 12(a) shows that on the non-seam side of the ball there is a white stripe caused by a flow separation. The flow separates at the front of this stripe and the recirculating flow, trapped beneath the separated shear layer, has low heat transfer so the surface of the ball remains cold. This result agrees with Scobie et al.'s sketch for the non-seam side shown in Fig. 11 and confirms that the separation angle on this side of the ball is approximately 80°. Figures 12(a)-(c) also show that the position of the laminar separation on the non-seam side does not change between $Re = 1.42 \times 10^5$ and $Re = 1.89 \times 10^5$. This agrees with Achenbach's result for a smooth sphere, Fig. 10, which shows that the separation angle remains constant at 82° for cases where Re is below the critical value.

Measurements using model balls instrumented with pressure tappings by Scobie et al. [14], see Fig. 9, and Deshpande et al. [22], have also shown that the separation on the non-seam side occurs at approximately 80°. Figure 8(d) from Jackson et al. [15] shows that the separation angle on the non-seam side at $Re = 1.1 \times 10^5$ is 95°. The authors explain that this is because the surface roughness is greater than a new ball and links this to Achenbach's roughened sphere results in Fig. 10. For the separation angle to increase to 95° implies that transition has begun but this idea is not discussed. It is also noted that the model ball tested by Jackson et al. is a replica of the one used for the measurements in Fig. 9. The roughness of these balls is reported to be the same, however, Scobie et al.'s tests at $Re = 0.20 \times 10^5$ and $Re = 1.47 \times 10^5$ both show a laminar separation at approximately 80°. The discrepancy between these results and the PIV result in Fig. 8(d) is not explained.

Seam side. Existing publications discussing cricket ball swing often state that the boundary layer on the seam side is 'tripped' to turbulence by the seam. Indeed, Horlock [9], Deshpande et al. [22] and Sayers [29] test model cricket balls where the seam is represented by a wire trip. Son et al. [30] describe two ways in which a wire trip can delay boundary layer separation and reduce drag: first, the disturbance

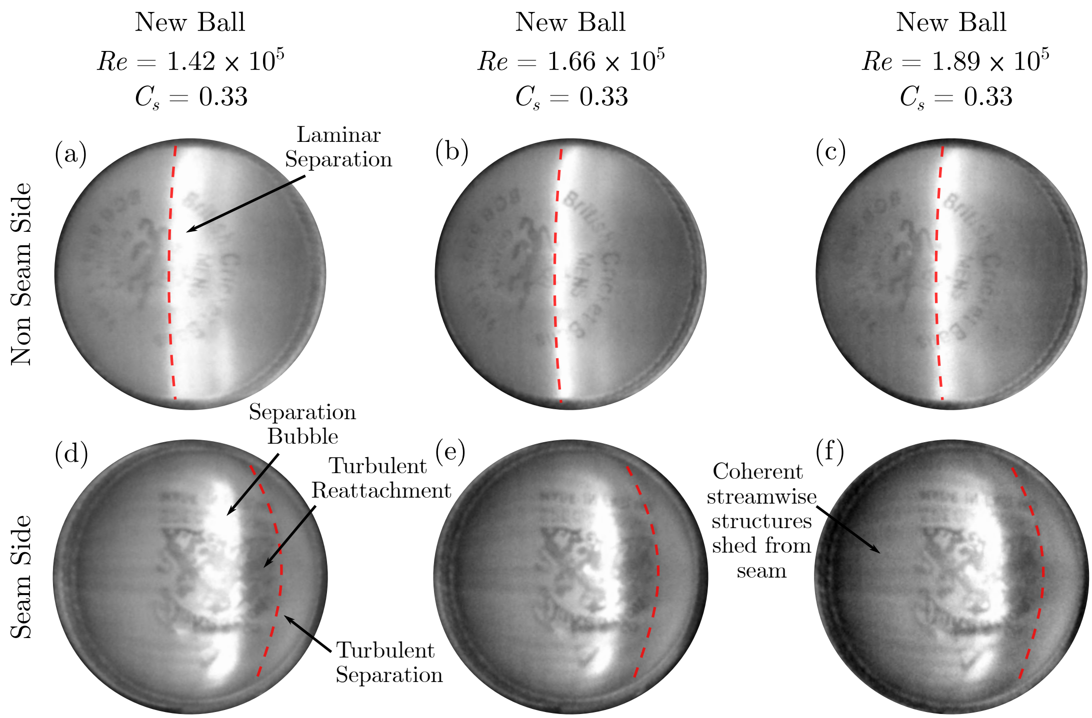

Figure 12. *Seam and non-seam side IR images of a new, red Dukes cricket ball, Ball I in Fig. 6, undergoing conventional swing at varying Reynolds Number. Flow is left to right and red dashed lines illustrate eventual separation position.*

from the trip can cause transition along the separated shear layer resulting in a a separation bubble and turbulent reattachment. Alternatively, disturbances from the trip can cause transition to turbulence before separation, with no separation bubble formed. Deshpande et al. are the only authors to suggest the presence of a laminar separation bubble on the seam side, while others state that the boundary layer is tripped with no mention of a separation bubble.

Another description of the flow on the seam side of the ball, provided by Scobie et al. [21] and Jackson et al. [15], links the seam side behaviour to the rough sphere in Fig. 10 (black line with square symbols) so that, for conventional swing, the seam side boundary layer separates further back on the ball than the smooth, non-seam side (red line). Achenbach's data for the rough sphere shows a separation angle of 100+/-5° in the range $Re = 1 - 2 \times 10^5$. However, Jackson's PIV measurement of a model cricket ball, Fig. 8(d), and Scobie et al.'s measurements using an instrumented model ball, Fig. 9, show a separation angle of 120+/-5°. This is the value used in the diagram in Fig. 11. The difference between the rough sphere and cricket ball experiments are not discussed and we conclude that Achenbach's rough sphere results are unsuitable for modelling the seam side of a cricket ball, since the separation angles differ by approximately 20°.

Figures 12(d)-(f) present Whittle Laboratory IR images of the seam side of the ball for conventional swing at varying Re. These results show streamwise 'streaks' on the front half of the ball which are caused by coherent structures shed by the seam. These appear dark in the image, where warm flow from the freestream is mixed down to the cool surface of the ball, implying that the seam acts more like a row of vortex generators than a wire trip. Just behind the midpoint of the ball there is a laminar separation bubble, indicated by the white stripe in the IR images. The separation bubble is closed with a turbulent boundary layer reattachment, shown by the dark region of high heat transfer, before the flow eventually separates towards the back of the ball.

The results in Fig. 12 show that streamwise flow structures are involved in the separation and reattachment of the boundary flow on the seam side. This type of behaviour is widely reported in the literature outside of cricket ball aerodynamics, and reviews are provided by Gad-el-Hak and Bushnel [31] and Yang [19]. Much of this 'boundary layer control' research is concerned with improving the performance of aircraft wings, however, Joubert et al. [32] show that vortex generators placed along a cylinder, 20° from the stagnation point, are able to reduce drag by 50% at $Re = 1.3 \times 10^5$ compared to a smooth cylinder. We hypothesise that the cylinder drag reduction measured by Joubert et al. is due to the same kind of flow physics seen in Figs 12(d)-(f): the coherent streamwise structures shed by the seam/vortex generators interact with the separated shear layer causing transition, a turbulent boundary layer reattachment, and eventual separation towards the rear of the ball/cylinder. This is different to the wire trip or rough sphere mechanisms where transverse perturbations cause the transition to turbulence.

Flow visualisation and pressure tapping measurements by Deshpande et al. [22] also indicate the presence of a laminar separation bubble on the seam side. However, these results appear to have been overlooked by other researchers since they are recorded using an aluminium model ball, where the switch from conventional to reverse swing does not occur until approximately $Re = 4 \times 10^5$, an unrealistically high value for cricket. Scobie et al.'s measurements in Fig. 9, show that at $Re = 1.47 \times 10^5$ (labelled CS - 67mph) there is a flattening of the pressure profile between 80° and 90° on the seam side. This is indicative of a laminar separation bubble, however this feature is not discussed in Scobie et al.'s paper [14] or the same group's subsequent work [21, 15].

Overall, the description of seam side flow for conventional swing, summarised in Fig. 11, where the seam is said to trip the boundary layer, should be updated. The IR images in Fig. 12, supported by previous pressure tapping measurements [22, 14], show that coherent streamwise structures are shed from the seam and that these cause a turbulent reattachment behind a laminar separation bubble.

Flow Asymmetry Combining the descriptions for the non-seam and seam sides leads to an updated explanation for conventional swing. Figure 13 shows a top down sketch of the flow past a cricket ball. The laminar separation on the non-seam side was hypothesised in the earliest papers on cricket ball swing in the 1950s and has been shown to occur at approximately 80° when *Re* is below the critical value for that side of the ball.

On the seam side, established explanations that the boundary layer transitions to turbulence because the seam acts like a wire trip, or that the seam side behaves like a rough sphere, should be revised. Figure 13 shows coherent streamwise structures, shed from the seam, which close a separation bubble and result in a turbulent boundary layer separation at approximately 120°.

The asymmetry in the boundary layer separation results in a sideways force which causes the ball to swing in the direction that the seam is pointing. While the non-seam side flow is below a critical *Re*, the separation points on both sides of a new ball do not change greatly for $Re = 1.42 \times 10^5$ to $Re = 1.89 \times 10^5$, as shown in Fig. 12. This explains why C_S, shown in Fig. 6 for new balls, does not vary significantly, e.g. for a new red Dukes ball, tested at the Whittle Laboratory, there is less than 5% variation in C_S between $Re = 1.42 \times 10^5$ and $Re = 1.92 \times 10^5$. Figure 7 shows that used balls can also exhibit conventional swing with C_S between 0.2 and 0.35, however, the switch to reverse swing occurs at lower *Re* and is less sudden than for new balls. This is because a roughened non-seam side transitions more gradually and at lower *Re*, as shown for rough spheres by Achenbach in Fig. 10.

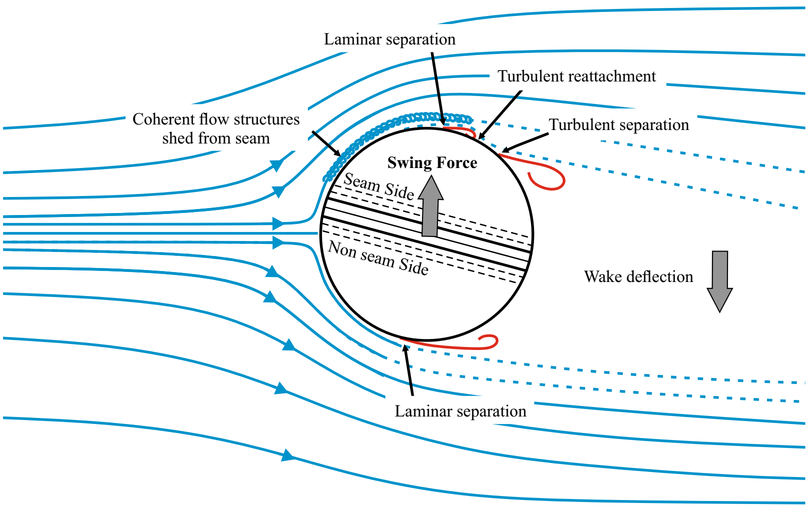

Figure 13. *Top down sketch of flow past a cricket ball for conventional swing updated using Whittle Laboratory results.*

4.2. Reverse Swing

Reverse swing occurs when C_S is negative so that the ball deviates away from the direction that the seam is pointing. Figure 6 shows that new balls, with *Re* above a specific value, have a negative C_S of -0.05 to -0.1. For old balls, shown in Fig. 7, reverse swing occurs at lower *Re* and C_S varies between 0 and -0.4.

The first reference in the literature to a behaviour now recognised as reverse swing was made by Horlock [9] who noted that "*The presence of the secondary* [quarter] *seam appears to cause transition on the smooth* [non-seam] *side in some cases and may cause small or even negative lift*". He explains that this is because *Re* is greater than the critical value on both the non-seam and seam side causing both to transition to turbulence. Mehta [10] builds on this idea and hypothesises that the seam causes the separation on the seam side to occur further forwards than the non-seam side which switches the direction of the swing force compared to conventional swing.

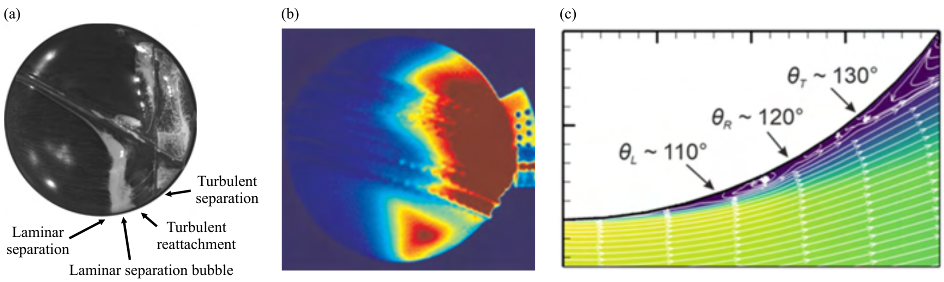

Figure 14. *Flow visualisation experiments from literature illustrating flow past the ball for reverse swing with flow moving from left to right. (a) Oil flow visualisation on an aluminium model ball at* $Re = 3.92 \times 10^5$ *[22]; (b) IR imaging of a model cricket ball at* $Re = 1.95 \times 10^5$ *[14]. Red indicates a separated region where heat transfer from the freestream flow to the ball is low; (c) PIV measurement of model cricket ball on non-seam side at* $Re = 1.74 \times 10^5$ *[15]. Yellow contours indicate high velocity, dark blue contours indicate zero velocity.*

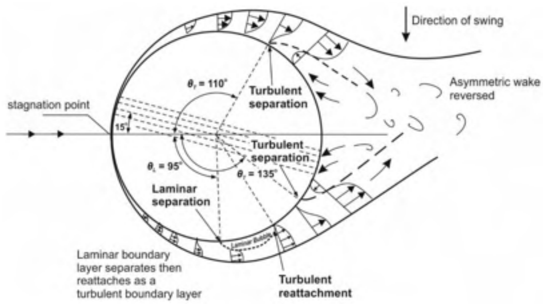

Figure 15. *Top down sketch of flow past a cricket ball for reverse swing. Reproduced from Scobie et al. [21].*

Further studies on reverse swing, reproduced in Fig. 14, have provided experimental evidence to support Mehta's idea. Deshpande et al. [22] show oil flow visualisation on an aluminium sphere with trip wire representing the seam as shown in Fig. 14(a), Scobie et al. [14] study a model ball using IR visualisation as shown in Fig. 14(b) and Jackson et al. [15] provide a top down view of the flow past a model ball using PIV as shown in Fig. 14(c). These results highlight the presence of a laminar separation bubble and turbulent reattachment on the non-seam side and Fig. 15, reproduced from Scobie et al. [21], consolidates these results to provide the most recent description of reverse swing.

Figure 7 shows C_S for old balls varying between 0 and -0.4. This is due to differences in the separation asymmetry between the two sides of the ball with the largest force obtained when the seam side separation is as far forward as possible, and the non-seam side separation is as far back as possible. The rest of this section reviews boundary layer behaviour on each side of the ball in order to assess the explanations given in the literature and to understand why reverse swing magnitude varies more than conventional swing. The literature review is supplemented by Fig. 16 which shows IR images captured in Whittle Laboratory experiments for three balls which have negative C_S.

Non-seam side. On the non-seam side, Fig. 15 shows that the laminar boundary layer separates at 95°, forms a laminar separation bubble, reattaches as a turbulent boundary layer and then separates to form a wake at 135°. This explanation is based on several measurements reported in the literature: Figure 9 shows that at $Re = 1.95 \times 10^5$ (89mph - RS), a constant pressure is recorded between -90° and -100°, indicating the presence of a separation bubble; Fig. 14(a) shows a laminar separation bubble

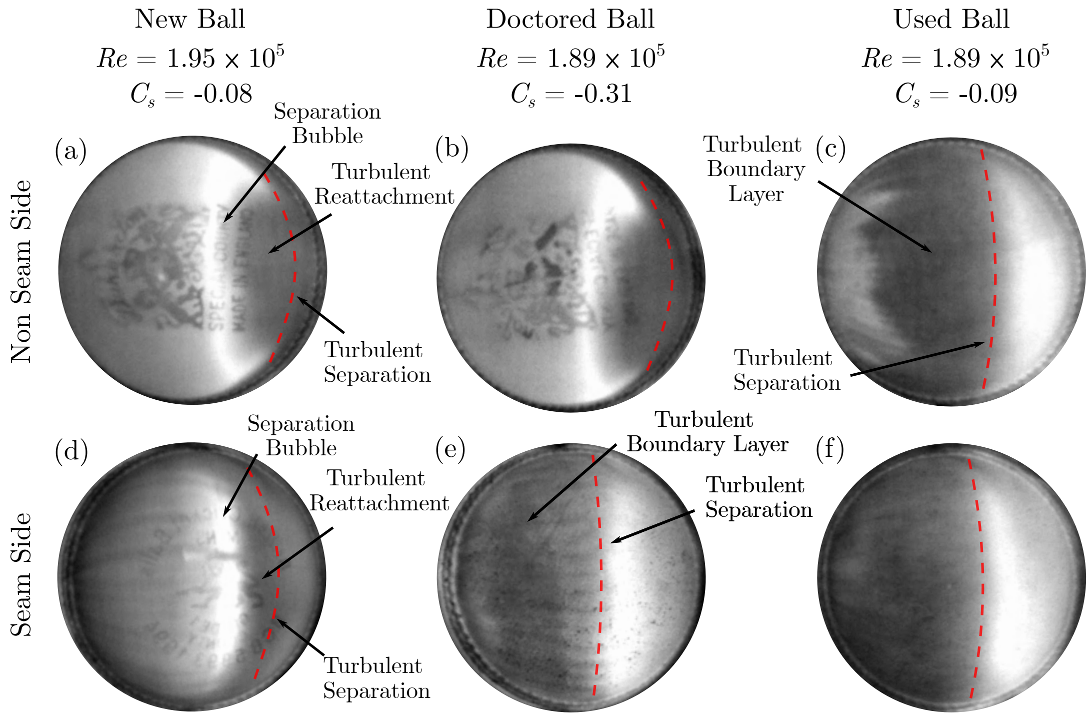

Figure 16. *Seam and non-seam side IR images of three cricket balls undergoing reverse swing. Flow is left to right and red dashed lines illustrate eventual separation position. (a) New ball with shiny seam and non-seam sides, Ball I in Fig. 6; (b) 'Doctored' ball with rough seam side and shiny non-seam side, Ball M in Fig. 7; (c) Used ball with rough seam and non-seam sides, Ball N in Fig. 7.*

on the non-seam side using oil flow visualisation; the red region on the non-seam side in Fig. 14(b) indicates a separation bubble and reattachment; and in Fig. 14(c) PIV measurements show a laminar separation, reattachment and eventual turbulent separation at 130°. The Whittle Laboratory IR image of the non-seam side of the new ball in Fig. 16(a) matches the flow mechanism sketched in Fig. 15: the white stripe followed by a dark region indicates a laminar separation bubble and turbulent reattachment. These results agree qualitatively with Achenbach's measurements [27] for smooth spheres above a critical Re of $2-3\times10^5$, shown in Fig. 10, where the flow becomes turbulent in the shear layer of the laminar separation, causing a turbulent boundary layer to reattach then finally separate at 120°.

Figure 16(c) shows an IR image of the non-seam side of a ball artificially roughened to represent an old ball. Roughness is generated with a sand blaster and is measured using a profilometer to be $k/D = 55\times10^{-5}$ for the cases shown in Figs 16(c), (e) and (f) where k is the peak-to-peak value of the surface profile. Further details of the generation and measurement of surface roughness are given in Appendix A. Visualisation for this condition has not been presented in the literature before, though force measurements for old or artificially roughened balls, are reproduced in Fig. 7. In Fig. 16(c), a region of laminar flow, which appears light grey because the heat transfer coefficient is low, is observed at the front of the ball. The surface roughness then causes the boundary layer to become turbulent, there is no laminar separation bubble, and the turbulent separation is moved forwards compared to the new ball case shown in Fig. 16(a). This behaviour is consistent with Achenbach's results in Fig. 10 where the separation angle for the rough spheres are 10-20° further forwards than for the smooth sphere for cases where Re is above the critical value.

Scobie et al.'s sketch of the non-seam side flow in Fig. 15 captures the case when the ball is new or its shine has been maintained. However, a second drawing is required to describe the non-seam side flow as the ball becomes older and more worn and the separation point moves forwards.

Seam side. Figure 15 shows a turbulent boundary layer separation on the seam side at 110° and this is also labelled on the pressure measurements shown in Fig. 9 for the RS (reverse swing) case. As with the conventional swing results, Scobie et al. [14] do not discuss the flattening of the pressure profile observed between 80° and 90° which suggests the presence of a laminar separation bubble.

The Whittle Laboratory IR image in Fig. 16(d) shows that the seam side behaviour of a new ball at $Re = 1.95 \times 10^5$ is similar to that in the conventional swing regime at $Re = 1.89 \times 10^5$, shown in Fig. 12, with streaks shed from the seam, a separation bubble, turbulent reattachment, and eventual separation. This is consistent with the flattened pressure profile between 80° and 90° seen in Fig. 9 for reverse swing.

Figures 16(e) and (f) show IR images of the seam side of the ball for cases where artificial roughening has been applied. Here, the roughness causes the boundary layer to be turbulent towards the front of the ball, there is no separation bubble and turbulent reattachment, and the separation point is moved forward compared to the new ball case shown in Fig. 16(d). This result is similar to the flow visualisation on the seam side shown in Figs. 14(a) and (b). The coherent structures shed from the seam are not as clear in Figs. 16(e) and (f) as the other seam side cases. This is because the rough surface causes a turbulent boundary layer to develop and the heat transfer coefficient is increased. This reduces the contrast in heat transfer caused by the coherent flow structures so the streaks are not as noticeable in the IR image. The geometry of the seam is not changed by the roughening process used here so flattening or damaging the seam is not responsible for the streaks being less visible and the changes in measured force coefficient.

Scobie et al.'s seam side sketch of the flow in Fig. 15 should be updated to include a laminar separation bubble for cases where the ball is new or its shine has been maintained. A second sketch is required to describe the seam side flow as the surface becomes older and more worn and the separation point moves forwards.

Flow Asymmetry. Measurements of swing force coefficient for old balls, collated in Fig.7, show that reverse swing magnitude varies more than conventional swing magnitude. This is due to the different conditions shown in Fig. 16 which 'bracket' the boundary layer behaviours that can occur on each side of the ball. To illustrate this, top down sketches of the flow are presented in Fig. 17 for the three cases recorded in Fig. 16.

For a new ball which reverse swings, the separation on both sides is towards the back; the seam side separation is slightly in front of the non-seam side resulting in a small C_S of -0.08. With the doctored ball, the separation point on the seam side is brought forward by roughness, increasing the asymmetry and resulting in $C_S = -0.31$. For the old ball, the separation on the non-seam side has also moved forwards meaning that the asymmetry is reduced so that C_S is only -0.09. This updated model for reverse swing, shown in Fig. 17, allows previous literature results, including real and model balls, to be reassessed and grouped.

Different brands of new ball tested by Scobie et al. [21] and Deshpande et al. [22], balls A-E in Fig. 6, have shiny seam and non-seam sides and C_S between 0 and -0.1 above a critical Re. The sketch in Fig17(a) captures these balls' behaviour.

The model ball tested by Scobie et al. [14] and Jackson et al. [15] has a laminar separation bubble on the non-seam side, as shown with pressure measurements in Fig. 9 and PIV in Fig. 14. No PIV visualisation of the seam side is provided, however, there is evidence in Fig. 9 of a laminar separation bubble as discussed above. The model ball's roughness is said to represent 25 overs of wear and C_S is measured to be between -0.12 and -0.18. Similarly, the 8-10 and 25 overs old balls, labelled A and B in Fig. 7, have C_S between -0.1 and -0.13 for $Re > 1.8 \times 10^5$. These balls are likely to sit somewhere between the sketches in Fig. 17 (a) and (b) where the laminar separation bubble on the non-seam side is present but the separation point on the seam side is moved forwards, compared to a new ball, due to roughness. For these cases, reverse swing magnitude could be increased by roughening the seam side more to bring the separation point further forward.

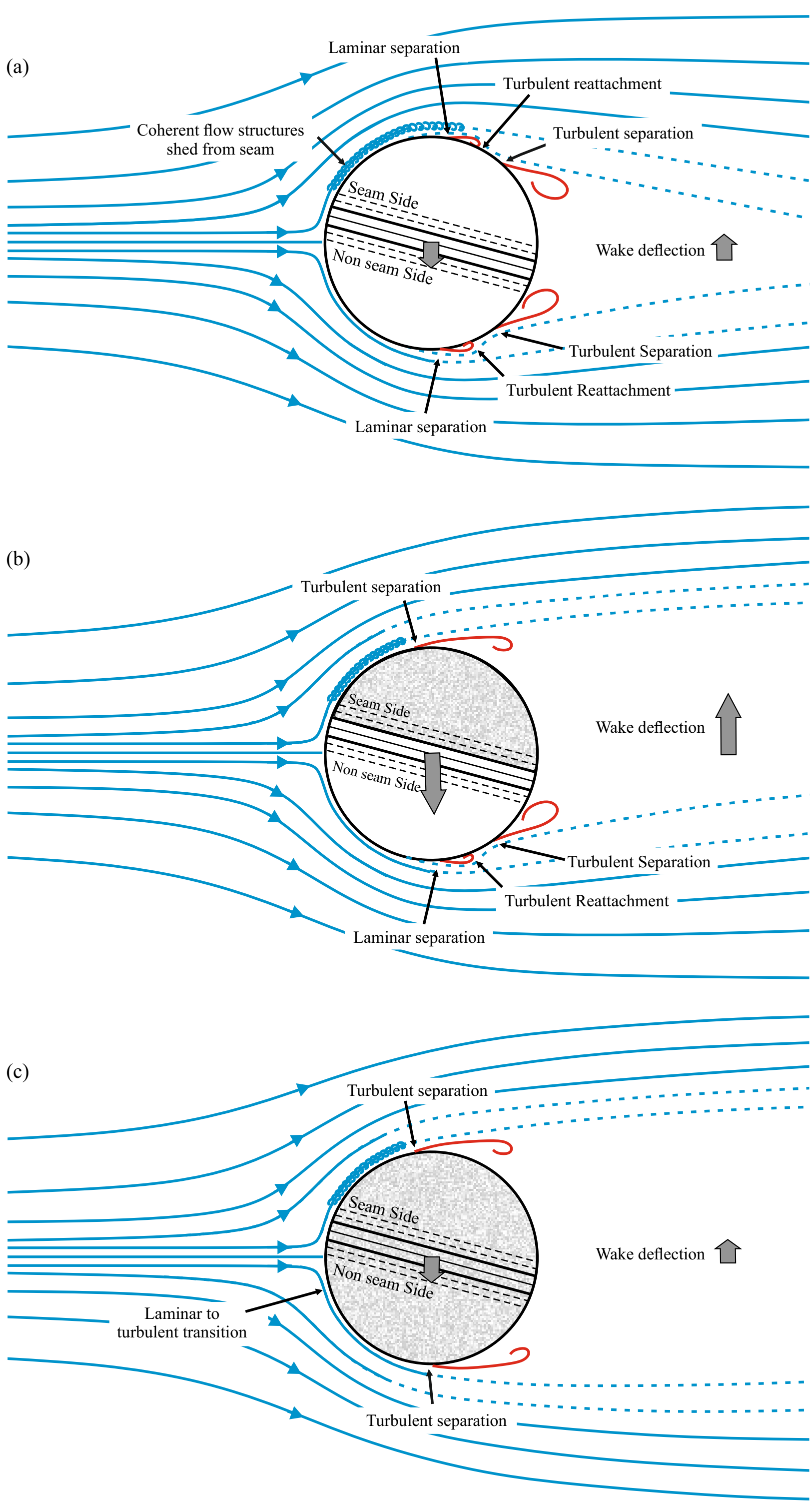

Figure 17. *Top down sketches of flow past a cricket ball for reverse swing updated using Whittle Laboratory results. (a) New ball with shiny seam and non-seam sides; (b) Doctored ball with rough seam side and shiny non-seam side; (c) Used ball with rough seam and non-seam sides.*

Deshpande et al. [22] also tested a seam side roughened ball, Ball H in Fig. 7, which has C_S around -0.2 for $Re > 1.95 \times 10^5$. This test is similar to the doctored ball shown in Fig. 16(b) so will have behaviour represented by the sketch in Fig. 17(b). Old balls provided by a professional cricket team and tested by Scobie et al. [14], Balls E-G in Fig. 7, have swing force coefficients between -0.2 and -0.3 and are likely to sit with this group as well. Tadrist et al. [25] measured swing force coefficients between -0.22 and -0.34 at $Re = 2.4 \times 10^5$ for cricket balls at 0° seam angle with one side roughened and the other left as new, Balls J and K in Fig. 7. These tests are also best represented by the sketch in Fig.17(b).

Old balls tested by Scobie et al. [21], have swing force coefficients between 0 and -0.1, for example Ball D in Fig. 7. Photographs of these balls show they are worn on both sides with prominent gaps in the quarter seam and they are therefore likely to behave as shown in Fig. 17(c). Deshpande et al. [22] tested a ball where both sides were artificially roughened, resulting in swing force coefficients between 0 and 0.1 for $Re > 2 \times 10^5$; this is Ball I in Fig. 7. The behaviour of this ball is best captured by Fig. 17(c), but where the non-seam side is rough enough to move its separation point in front of the seam side, causing a small, positive swing force.

Our updated model allows reverse swing magnitude to be linked to a range of ball conditions. However, the quantified relationship between surface roughness, Re and separation angle on both sides of the ball, has not been investigated systematically and this represents an area for future work.

4.3. Switch from Conventional to Reverse Swing

Figure 6 shows that the switch from conventional to reverse swing for a new ball measured in a wind tunnel occurs with a change in Re of less than 5%. This is due to the sudden increase in separation angle on the non-seam side as flow changes from the sub critical to super critical regime. Figures 6 and 7 also show that there is variation in Re at which the change occurs, with old balls switching at $Re < 1.5 \times 10^5$ and new balls switching at up to $Re = 2.15 \times 10^5$.

Differences in experimental setup from study to study are likely to account for some of the variation observed, e.g. how the ball is mounted, blockage factor and freestream turbulence intensity of the wind tunnel. However, different balls tested by Scobie et al. [21] are assumed to share the same setup, and this is also the case for balls tested at the Whittle Laboratory for this paper.

Surface roughness changes Re at which the laminar separation on the non-seam side reattaches, as shown in Fig. 10 for spheres with different levels of roughness. Jackson et al. [15] estimate that the roughness of a new ball is in the range $0 < k/D < 250 \times 10^{-5}$. Tadrist et al. [25] repeatedly measure the surface roughness of a ball as it is used. Values of $k/D = 8.5 \times 10^{-5}$ are reported for a new ball and this increases to $k/D = 100 \times 10^{-5}$ as it becomes worn. A new, red, Kookaburra ball measured at the Whittle Laboratory has $k/D = 14 \times 10^{-5}$ on the lacquered surface, while the artificially roughened ball shown in Fig. 16 has $k/D = 55 \times 10^{-5}$. Balls made by Kookaburra, Dukes and SG are lacquered when new and not expected to have significantly different levels of surface roughness, though this should be quantified. The different brands have different seam geometries, however, this does not affect the switch from sub critical to super critical regimes on the non-seam side. Despite this, the results in Fig. 6 for new ball swing show a variation in Re at which the switch from conventional to reverse swing happens of $Re = 1.8 \times 10^5$ - 2.15×10^5.

As well as uniform surface roughness, new cricket balls have small 'defects' on both sides of the ball. Horlock [9] comments that the quarter seam can cause boundary layer transition on the non-seam side and Bentley et al. [28] also identify the quarter seam and logo as features which increase the "*effective roughness*" of the ball. More recently, Scobie et al. [21] compared three types of new ball using the same experimental setup; these results are reproduced in Fig. 6. They comment that the difference between the red and pink Dukes balls are "*probably caused by slight differences in the surface texture*", while the most prominent difference with the white Kookaburra, which switches from conventional to reverse at a lower Re, is due to "*a prominent secondary seam* [quarter seam]" which has a 0.5mm gap. These existing discussions of surface condition are mainly qualitative, therefore quantifying cricket ball surface roughness and defects, and establishing a relationship to Re at which conventional swing switches to reverse swing should be an area for future study.

The effect of defect position on cricket ball swing has not been studied, however, Schewe [33] investigated the sensitivity of boundary layer flow to small perturbations close to critical Re, on a cylinder. The boundary layer across the entire cylinder length was made to transition by protruding a pin, with a height 1% of the cylinder diameter, into the flow at the centre of the cylinder. For transition to occur reliably, the pin had to be positioned at ϕ_s=45-60°. Schewe concludes that "... *in the vicinity of a critical state, a very small cause can have a very great effect*", indicating that small defects on a cricket ball can be expected to switch the whole flow regime if they are in the correct location on the ball.

Sayers and Hill [23] show a variation in swing force of approximately 15% for seam angles of 10°, 30° and 50°. However, these wind tunnel tests are performed at $Re < 1.7 \times 10^5$ which is not high enough to show the effect on non-seam side transition. Deshpande et al. [22] test a new cricket ball at 10°, 20° and 30° and show that the 10° and 30° cases switch from conventional to reverse swing at Re within 5% of each other. However, the 20° case switches at Re around 35% below the 10° case. Similar results are presented by Shah and Mittal [34] who report a variation of approximately 25% in Re at which the switch occurs for cases with seam angles of 10° and 20°. Neither paper provides an explanation for this behaviour, however, we hypothesise that differences observed at specific seam angles are due to a defect on the ball moving to a position which causes early transition.

Barton [35] measures C_S for a new ball and a ball used for 10 overs at seam angles of 15° and 30° up to $Re = 1.32 \times 10^5$. For the new ball, increasing seam angle reduces the peak C_S from 0.36 to 0.31 and reduces Re at which the sudden drop in C_S occurs. The same trends are observed for the 10-over old ball though C_S is reduced compared to the new ball. An additional test at seam angle of 0° for the 10-over old ball results in a maximum C_S of 0.38. For this case, Barton concludes that the quarter seam, oriented perpendicular to the flow direction on one side of the ball, is sufficient to trip the boundary layer and cause the flow asymmetry needed for swing. Bentley et al. [28] perform a wind tunnel study using a cricket ball with pressure taps and also conclude that the pressure difference between each side of the ball, and hence swing magnitude, is reduced if the quarter seam on the non-seam side is perpendicular to the flow direction. Since Barton and Bentley's studies were published in the early 1980's, little attention has been paid to the effect of rotation angle, α, on the magnitude of C_S and Re at which the switch from conventional to reverse swing occurs.

The results in Fig. 6 show that the switch from conventional to reverse swing for a new ball is sudden and that C_S between 0 and 0.2 are rarely recorded. This contradicts ball tracking data for new balls in Fig. 2, which shows that in practice there is a continuous distribution. Previous work does not explain this discrepancy, however, the sensitivity of the non-seam side boundary layer behaviour to small defects or quarter seam orientation suggests a new hypothesis: as the ball rotates, the seam angle varies and defects change position; this can change the swing from conventional to reverse at constant Re and averaging the force between these states explains how C_S between 0 and 0.2 occur.

In discussing the variation between new balls, Scobie et al. [21] suggest that "... *a larger number of samples is required to further the investigation.*" Our review supports this statement and also concludes that future work should systematically vary both seam angle, θ, and rotation angle, α, for each ball tested, so that rotation can be modelled and the hypothesis around averaging investigated quantitatively.

4.4. 2D Approximation

Explanations of swing in the literature and in this paper assume that the flow past a cricket ball can be considered two-dimensional. In developing his cricket ball trajectory model, Baker [20] asks whether this is "... *a little too simplistic: they* [papers in the literature] *implicitly relate the flow around a three-dimensional (3D) sphere to that around a 2D cylinder in terms of boundary layer behaviour, although it is by no means clear that the boundary layer would behave in precisely the same way*". Baker's paper was published in 2009 and since then the flow visualisation experiments shown in Figs 8 and 14, performed by Scobie et al. [14], Jackson et al. [15] and Deshpande et al. [22], along with the new

IR images presented in this paper, show that the separations on cricket balls are predominantly two-dimensional. This observation is supported by Taneda [36] who reports that the wake behind a smooth sphere collapses to a two dimensional plane.

4.5. Summary

Previous research relating cricket ball swing with boundary layer aerodynamics has been supplemented with new wind tunnel experiments which include IR imaging to visualise the boundary layer flow. Explanations for conventional and reverse swing have been updated and are summarised here, along with areas for future study.

Conventional swing occurs because the flow separates further back on the seam side of the ball than the non-seam side. This deflects the wake to the side causing a reaction force on the ball which results in swing. For this asymmetric flow to be established, the non-seam side boundary layer has to remain laminar so that it separates at approximately 80°. On the seam side, streamwise coherent structures are shed from the seam and interact with the free shear layer downstream of a laminar separation, leading to a turbulent reattachment of the boundary layer which then separates with a turbulent separation at approximately 120°.

Reverse swing occurs when the flow asymmetry is switched and the flow separates further back on the non-seam side than the seam side. For a new ball, this occurs when Re is high enough to cause transition on the non-seam side so that the laminar separation reattaches as a turbulent boundary layer before separating at approximately 135°. The seam side flow, for a new ball, is similar to the conventional swing case. The resulting difference in separation points on each side of the ball is reduced compared to the conventional swing case meaning the magnitude of C_S is three to four times smaller than for conventional swing with a new ball.

To maximise reverse swing, the seam side should be roughened while keeping the non-seam side as smooth as possible. This causes the laminar separation bubble on the seam side to close and the turbulent separation to move forwards, increasing the difference between the separation points on each side of the ball. If the non-seam side also becomes rough, its laminar separation bubble closes and the separation point moves forwards meaning that there is less flow asymmetry and reverse swing is reduced.

The switch between conventional and reverse swing occurs when the non-seam side flow changes from the sub critical to super critical regimes. This occurs at a specific Re which varies depending on the ball condition and orientation. However, the effect of surface roughness and defects, and their interaction with the seam and rotation angle, have not been studied in detail. Similarly, the link between surface roughness, Re, separation angle and reverse swing magnitude has not yet been quantified. Both of these topics should be an area for future work so that the effect of ball condition on conventional and reverse swing can be better understood.

The research reviewed in this section focuses on cricket ball boundary layer aerodynamics and the experiments considered were performed using a fixed mount in a wind tunnel. The following section studies the literature relating to the boundary conditions found in professional cricket, and how they may differ from the wind tunnel experiments already discussed. The effects of ball rotation and atmospheric conditions are reviewed and discussed with respect to the ball tracking data presented in the Introduction.

5. Realistic Boundary Conditions

The boundary conditions which determine whether a cricket ball will swing can be grouped into three categories: the condition of the ball, the kinematics of the delivery, and the properties of the air through which the ball travels, often called atmospheric conditions. Ball condition includes surface roughness, details of any defects including the quarter seam, and the geometry of the primary seam. The kinematics of the delivery are determined by the bowler and are characterised by Re defined in Equation 2, the seam angle, θ, the rate of change of seam angle, $d\theta/dt$ and the rotation rate, ω. The properties of the air are split into 'macroscopic conditions' which change slowly with time and which can be considered constant around a cricket ground, and ‘transient conditions’ which vary quickly, on the time scale of a delivery or shorter, and which are local to the air the ball is passing through.

The previous Section reviews the effect of ball condition, Reynolds Number and seam angle, variables which can be tested in a wind tunnel using a cricket ball mounted on a sting. This Section reviews ‘realistic’ boundary conditions, with papers studying the effect of ball rotation considered in the first subsection and work on atmospheric conditions in the second. As in the previous section, measurements reported in the literature are supplemented with experiments carried out for this paper.

5.1. Ball Rotation

Cricket balls delivered by swing bowlers are released with backspin about an axis approximately perpendicular to the plane of the seam as shown in Fig. 3. Bowling the ball so that its axis of rotation is precisely perpendicular to the seam requires skill and when this is not achieved the seam ‘wobbles’ so that seam angle, θ, varies throughout the ball’s flight. The rotation rate, ω, varies from bowler to bowler and is estimated from slow motion video footage to be in the range 5-15Hz. This subsection is split into three parts: the first reviews work where the ball is mounted on a spinning mount in a wind tunnel, the second considers two investigations where a spinning ball is dropped through the free jet of a wind tunnel, and the third examines studies using computational fluid dynamics (CFD) which include ball rotation.

Spin Mounted Wind Tunnel Tests. Rotating a cricket ball in a wind tunnel requires a mounting point to be located on the axis of rotation in the centre of the non-seam and/or seam side. This interferes with the boundary layer aerodynamics in an important region of the ball and limits the useful measurements which can be taken. Sayers and Hill [23] performed this type of experiment with a rotating mount passing through both sides of the ball. Their results show that at 30m/s and 0° seam angle, lift force, which acts perpendicular to the swing and drag forces, increases from less than 0.1N at 0Hz rotation rate, to between 0.3N and 0.45N at 8.3-16.7Hz, with these forces only “*weakly dependent on the speed of rotation*”. These results are explained by the Magnus effect which causes balls in tennis, baseball, football and golf to curve in the air, as described in [37, 38, 39, 40, 10]. Mehta [12] discusses how slow bowlers, as well as unusual side-arm bowlers, are able to use the Magnus effect to make cricket balls deviate laterally, but these phenomena are not the focus of this review. Further tests by Sayers and Hill, on drag and swing force, are limited by the parasitic force and disruption to the boundary layers caused by the mounting system for rotation.

Jackson et al. [15] test a rotating, twice scale model cricket ball which is mounted on one side. No force measurements are recorded and instead a PIV system is used to visualise the flow past the ball in two planes: from below, so that the non-seam side flow can be observed while the ball rotates, and

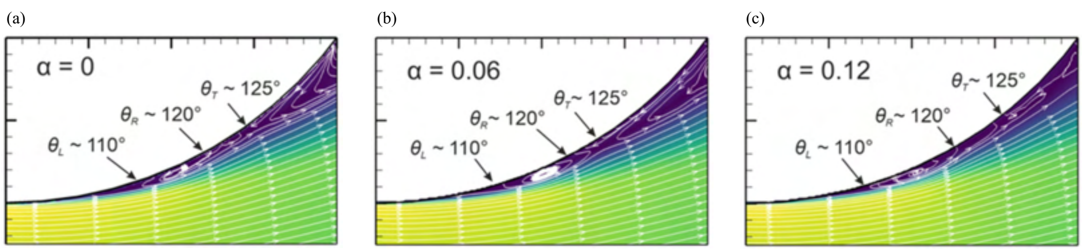

Figure 18. *PIV time-averaged velocity magnitude and streamlines on non-seam side at Re* = 1.69×10^5 *and seam angle 15° for varying spin rates. Separation and reattachment angles shown to nearest 5° [15] with (a)* $\alpha_{Jackson} = 0.0$*; (b)* $\alpha_{Jackson} = 0.06$*; (c)* $\alpha_{Jackson} = 0.12$*. Yellow contours indicate high velocity, dark blue contours indicate zero velocity*

from the side, so the flow in a plane aligned with the seam can be investigated in relation to the Magnus effect. A non-dimensional spin rate based on the ratio of tangential velocity at the top and bottom of the ball to the ball speed is defined: $\alpha_{Jackson} = 0.5\omega D/U$, using the nomenclature given in Fig. 3.

Jackson et al.'s results, reproduced in Fig. 18, show that the laminar separation, turbulent reattachment and turbulent separation on the non-seam side are unaffected by spin rates of $\alpha_{Jackson} = 0 - 0.12$ with $Re = 1.69 \times 10^5$ and seam angle 15°. This result refutes a hypothesis by Mehta [12] that rotation will stop the laminar separation bubble from forming. The second set of Jackson et al.'s tests, less relevant for this review, provide flow visualisation for the Magnus effect and support the results of Sayers and Hill which show how backspin generates lift.

Projection Wind Tunnel Tests. In 1982 two pieces of work were published which overcame some of the challenges of testing rotating cricket balls in a wind tunnel. Barton [35] and Bentley et al. [28] both performed experiments in which a cricket ball was rolled down an inclined track before dropping through the open jet of a wind tunnel. The ball spin rate was set by the distance rolled and the seam angle adjusted by moving the track angle relative to the direction of the wind tunnel jet. The forces acting on the ball were calculated by measuring the position that the ball lands relative to a datum and using trajectory equations. Both studies report results for a range of variables: Barton tested 17 different balls at 8 speeds up to 30m/s (67mph, $Re = 1.45 \times 10^5$), at seam angles of 0°, 15° and 30°, and at spin rates of 2.1Hz, 4.9Hz and 9.3Hz, while Bentley et al. tested 23 balls in total, of which 5 were tested at 7 speeds up to 40m/s (89mph, $Re = 1.93 \times 10^5$), at seam angles of 0°, 10°, 20° and 30° and at spin rates of 0Hz, 2.6Hz, 5Hz, 9.1Hz, 11.4Hz and 14.2Hz. Barton also qualitatively investigated the effect of seam wobble and Bentley et al. conducted experiments with a turbulence grid, discussed in the next Section on atmospheric conditions.

Barton and Bentley et al.'s projection tests are inherently less repeatable than stationary wind tunnel experiments and a spread of results is reported. Barton notes that some of the scatter is due to the method of projection: with the wind tunnel turned off, the balls land inside a strip 0.043m wide, 43% of the maximum deflection recorded when the wind tunnel was operating. On the other hand, Bentley et al. show that 4 pairs of balls "*of the same quality*" have force coefficients which vary only 6% on average at 30m/s with seam angle 20° and spin rate 5Hz. Both studies acknowledge the uncertainty in their results, however, through repeated tests and averaging, trends are observed and conclusions drawn.

Figure 19 is processed from projection test data published in Bentley et al. for two cricket balls released at 20° seam angle. Bentley et al. plot results with force normalised by ball weight against tunnel velocity in m/s and spin rate in Hz. This data is reprocessed in Fig. 19, assuming standard atmospheric conditions, to show contours of C_S against Re and reduced frequency. Reduced frequency for a spinning cricket ball is defined as the ratio of time taken for the flow to pass the ball to the time for the ball to complete a rotation. At a spin rate of 15Hz and speed 30m/s, $RF = \omega D/U = 0.035$, i.e. there are 28 flow through times for each revolution of the ball.

C_S for Ball 11, shown in Fig. 19(b), are positive across the range tested because Re is not high enough to cause transition on the non-seam side of the ball. However, for Ball 8, Fig. 19(a), the change from conventional swing to reverse swing occurs over a Reynolds number range of approximately 0.3×10^5. These results indicate a more gradual switch from conventional to reverse swing[1] than the sharp change seen in stationary wind tunnel tests plotted in Fig. 6.

Both Bentley et al. and Barton discuss which type of cricket ball is most likely to swing and they agree that a smooth non-seam side is required to maintain a laminar boundary layer for conventional swing. For example, Barton highlights a new ball with a "*gaped*" quarter seam which has an average $C_S < 0.2$ and Bentley et al. find that a two-piece ball, constructed without quarter seams, has the highest overall swing magnitude when C_S is averaged over a range of speeds, angles and spin rates. Both studies agree that the quarter seam, which Bentley et al. measure to be typically 0.1mm wide and 0.3mm deep,

[1]The term 'reverse swing' was not in use in the early 1980s, however, Bentley et al. note the negative force coefficients measured at high Reynolds number and include a private communication from Imran Kahn, a well known Pakistani cricketer, who confirms that he had observed the effect in practice.

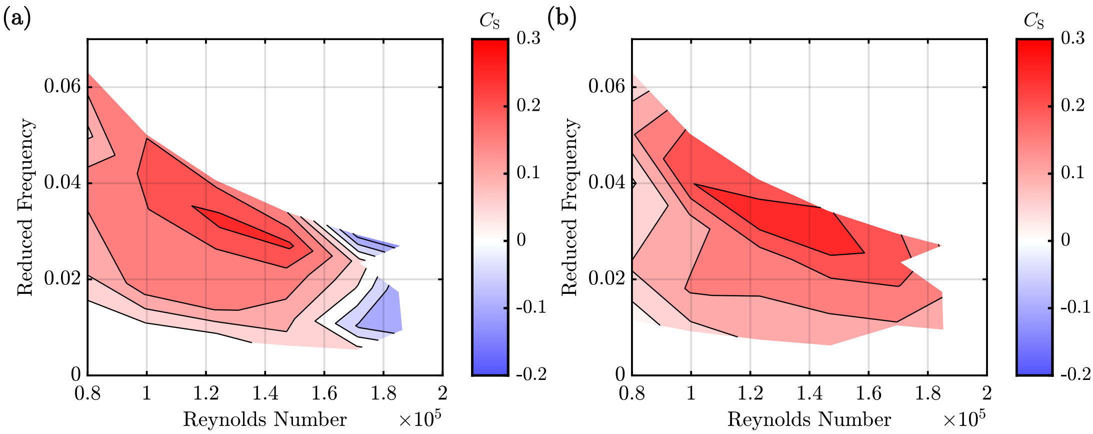

Figure 19. *Swing force coefficient, C_S, against Reynolds Number, Re, and Reduced Frequency reprocessed in non-dimensional form from data presented in Bentley et al. [28] for two balls at seam angle 20° with (a) Ball 8 and (b) Ball 11.*

as well as other features such as scuff marks and logos, produce an "*effective roughness*" when the ball is spinning. This causes transition on the non-seam side which stops conventional swing. Barton and Bentley et al. also test balls with different types of primary seam and while Barton suggests that balls with a "*prominent*" seam swing more, Bentley et al. state that seam "*stitching type*" is not as important as the smooth surface on the non-seam side.

The results reproduced in Fig. 20 are from the average of five different balls at seam angles of 10° and 20°. Again, the data is reprocessed to show C_S against Re and reduced frequency. It is observed that swing is maximised at a seam angle of 20°, $Re = 1.22 \times 10^5$ (25m/s, 56mph), and reduced frequency 0.033 (spin rate of 11.4Hz). In a similar analysis, Barton recommends a "*moderate*" spin rate of 5-8Hz and "*slight*" seam angle of 10-15° to maximise swing. Hypotheses to explain variation in swing with seam angle are discussed in Section 4.3, however, the effect of spin rate on swing has not been measured experimentally in any other work in the literature. Both papers note that spin helps to make the ball more stable and qualitatively observe that balls with zero or low spin rate (< 5Hz) wobbled more as they fell through the wind tunnel jet. Barton shows that increasing ball wobble reduces measured swing force and Bentley et al. state "*It is almost always the difficulty in maintaining stability that is responsible for a new ball not swinging*". Both studies therefore suggest that increasing spin rate up to a point improves ball stability and this increases swing.

To explain the optimum spin rate, Bentley et al. state that "*too much spin is of course detrimental since the effective roughness on the ball's surface is increased*" and a similar argument is made by Barton, though in this discussion it is also hypothesised that "*high rates of spin would almost inevitably be accompanied by wobbles and these too appear to diminish swing*". The idea that "*effective roughness*" is increased by spin rate is not investigated further in these studies or anywhere else in the literature and it is not clear what physical mechanism is involved. Figure 20 also shows that the average swing coefficient is higher at seam angles of 20°. This is consistent with the idea that seam wobble reduces swing if it causes the seam angle to vary above and below 0° during a delivery, effectively switching the seam and non-seam side. For a given amount of seam wobble, increasing seam angle reduces this effect as the mean angle is further from 0°.

The maximum reduced frequency in the tests is 0.063 and this drops below 0.04 for $Re > 1.22 \times 10^5$ (25m/s, 56mph). This implies that the problem is quasi-steady, i.e. the flow through time is more than an order of magnitude quicker than the rotation time so that spin rate should not be an important factor. Separating the effects of mechanical stability and aerodynamics using the projection tests was difficult for Barton and Bentley et al. and it is also not clear if the trajectory equations used account for varying

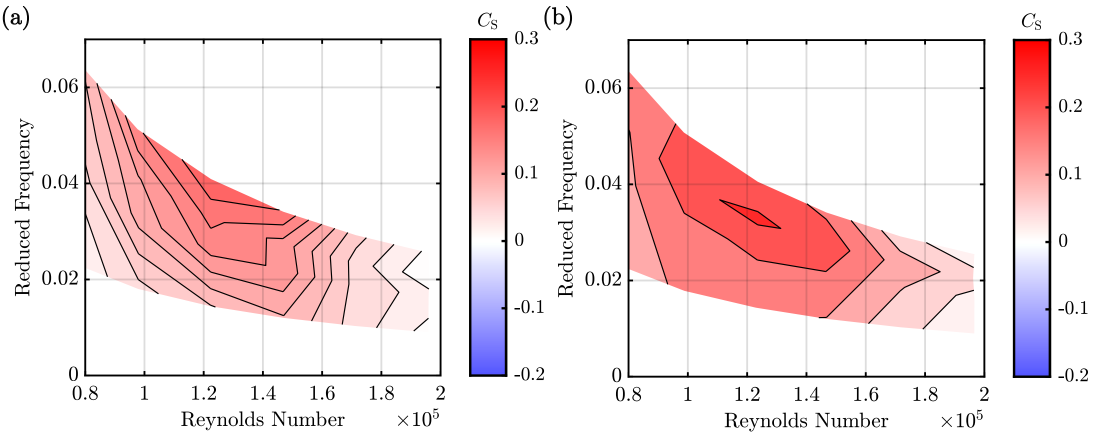

Figure 20. *Swing force coefficient, C_S averaged from 5 balls against Reynolds Number, Re and Reduced Frequency reprocessed in non-dimensional form from data presented in Bentley et al. [28] for two seam angles of (a) 10° and (b) 20°.*

lift on the ball, caused by Magnus effect changing with spin rate. Further work is required to confirm whether there is an optimum spin rate for cricket ball swing, and if there is, what mechanisms are responsible.

Barton and Bentley et al.'s projection tests, which include spin, are a more realistic representation of deliveries bowled in cricket matches than wind tunnel tests with cricket balls held in a fixed mount. This can be seen in the results in Figs 19 and 20 which show continuous distributions of C_S, more like the ball tracking data in Fig. 2, than the results from fixed tests in Fig. 6. We hypothesise that this is due to two effects: first, for each spinning projection test, rotation angle, α, and seam angle, θ, vary continuously so the flow past the ball can switch between conventional and reverse swing states and the swing force is averaged out to an intermediate value. Second, from test to test (or in a match, delivery to delivery) the seam angle and wobble can vary, along with the condition of the ball, resulting in a distribution of C_S for a given Re which when averaged give the smooth distributions seen in Fig. 2. Barton and Bentley et al.'s work illustrates this behaviour but further work is required to develop a statistical model which can quantify the effect of realistic boundary conditions including ball condition, seam angle and seam wobble. The optimum spin rate, observed by Barton and Bentley et al., is not understood and future work could repeat the projection tests using motorised, computer-controlled mechanisms for spinning and dropping the balls, and modern high-speed cameras for tracking their trajectory.

CFD Simulations. CFD can be used to simulate cricket ball swing where backspin is modelled using a rotating interface and unsteady calculation. Latchman and Pooransingh [41] simulate a cricket ball with a simplified geometry in which the primary seam is represented as a 20mm wide concentric rim projecting 1mm from the ball surface. Quantified details of the mesh, e.g. cell count and surface $y+$ are not provided. The solver used to simulate the flow is an incompressible, Reynolds-Averaged Navier-Stokes (RANS) scheme with $\kappa - \epsilon$ turbulence model. The ball was modelled at velocities from 22-45m/s, at seam angles of 10°, 20° and 30°, and with rotation rates from 0-14Hz. At 20°, increasing rotation rate from 0 to 2Hz increases C_S by 11% but for the cases between 2Hz and 14Hz there is less than 2% variation. Without rotation, C_S of 0.11, 0.21 and 0.39 are reported for 10°, 20° and 30° respectively. This result does not agree with the experimental results reviewed elsewhere in this paper and no explanation is given for the increase in C_S with seam angle. There is also less than 1% change in C_S across the full range of velocities simulated for each seam angle and overall these physically unrealistic results lead the authors to conclude "*that the $\kappa - \epsilon$ turbulence model may not be suitable for simulating the fluid flow around a cricket ball or that the model constants need to be redefined for this application*".

A similar study using RANS with a $\kappa - \epsilon$ turbulence model is reported by Kalburgi et al. [42]. This work shows the boundary layers separating further forward on the non-seam side than the seam side with a seam angle of 20° at velocities of 25, 29 and 36.5m/s. Similar to Latchman and Pooransingh's work, however, the switch from conventional to reverse swing associated with transition on the non-seam side is not captured. Kalburgi et al. do not quantify swing force from their calculations and do not model rotation.

Pahinkar and Srinivasan [43] report CFD simulations of reverse swing using a simplified geometry, similar to that of Latchman and Pooransingh [41]. Steady and unsteady RANS solutions are obtained using a Spalart-Allmaras turbulence model near the wall surface with Large Eddy Simulation (LES) in the freestream flow. The results show that for the velocities simulated, from 24-42m/s, the force is negative and surface pressure plots show that this is because the flow separates further forwards on the seam side than the non-seam side. The pressure plots do not show any evidence of laminar separation and turbulent reattachment on either side of the ball and negative C_S at all velocities indicates that this study is unable to capture transition on the non-seam side of the ball. Including ball rotation in the simulation increases the swing force magnitude but this effect is not explained.

Tom et al. [16] simulate cricket balls with smooth and rough surfaces where the rough surfaces have $k/D = 100 \times 10^{-5}$. There is no explanation of how these rough surfaces are implemented and details of the overall numerical scheme and mesh are not provided. Validation of CFD cases for conventional and reverse swing against "*real life*" trajectory data is shown to be within 0.01m throughout, though the source of the validation data is not provided. For conventional swing the ball is displaced $s = 0.29m$ over a delivery length of $l = 12.53m$ and using Equation 3 the average swing force coefficient is calculated to be $C_S = 0.237$. The paper goes on to study the behaviour of a new ball, where both sides are smooth and the rotation rate is 6.4Hz, and an old ball, where one side is smooth and one rough, and the rotation rate is 9.5Hz. C_S and C_D are reported for cases at various seam angles and speeds and for the new ball a maximum magnitude of $C_S = 0.05$ is reported. It is not clear how these results are made consistent with the trajectories reported in the validation section. Further details of the flow, such as the boundary layer states and separation points, and an explanation of the CFD setup, are not provided so it is not possible to assess how well the simulations match reality.

The studies reviewed in this subsection show that CFD can be used to investigate the effect of spin rate on swing. However, predicting cricket ball swing with CFD has proved challenging and to date, only simplified geometries have been simulated with models used to represent surface roughness. The sub and super critical flow regimes on the non-seam side of the ball also have to be captured accurately using the same turbulence modelling scheme so that the switch from conventional to reverse swing can be predicted. Only Tom et al.'s [16] results demonstrate this behaviour but unfortunately their paper does not provide information about CFD setup or detailed analysis of the flow. In conclusion, a comprehensive study of cricket ball swing using CFD has yet to be published and no agreed or established approach has been presented. This represents a significant area for future work.

5.2. Atmospheric Conditions

Cricket is played outdoors and the air that the ball encounters is subject to different atmospheric conditions. Cricketers and pundits believe that these conditions affect swing and tactical decisions can be influenced by weather conditions. For example, Australian fast bowler Mitchell Johnson noted that "*When there was cloud cover they [England] would attack, anticipating that the ball would swing. When the sun shone, they looked to tie us down, apply a more defensive approach.*" [44] .

Literature relating to the atmospheric conditions affecting cricket can be split into two categories: 'macroscopic conditions' which change slowly and which can be considered constant around a cricket ground, and 'transient conditions' which vary quickly, on the time scale of a delivery or shorter, and which are local to the air the ball is passing through. Published work relating to these categories is reviewed below.

Macroscopic Conditions. These are atmospheric conditions which change slowly during play and which affect a whole cricket ground uniformly. 'Slowly' means that properties can be considered constant through periods of play of the order an hour long. Properties which affect the cricket ball on this timescale are atmospheric temperature, pressure and humidity. Cricketers often talk about 'cloud cover' but this is not included in this discussion as it is difficult to quantify and does not directly affect the air flow around the ball. However, the relationship between cloud cover and other variables will be considered where relevant.

The Reynolds number, Re, defined in Equation 2, is a function of air density and dynamic viscosity, quantities which are affected by the macroscopic properties listed above. The density and viscosity for humid air can be calculated from pressure, temperature and humidity using formulae from Tsilingiris [45]. For example, an increase in air temperature from 25°C to 35°C, with fixed atmospheric pressure of 101.2kPa, reduces Re for a ball delivered at 40m/s (89mph) from 1.85×10^5 to 1.74×10^5, a decrease of 6%. For a match played at an altitude of 1500 m, as is the case at Centurion in South Africa, the atmospheric pressure is reduced to 85kPa. Here, at a fixed temperature of 25°C, a 40m/s delivery has $Re = 1.58 \times 10^5$, a decrease of 15% compared to the case at standard sea level conditions. Finally, for the case with 25°C and atmospheric pressure of 101.2kPa, increasing relative humidity from 0% to 90% increases Re from 1.85×10^5 to 1.86×10^5, an increase of 0.6%. These results show that changes in temperature and pressure should be taken into account when the bowling speed is converted to Re, however, the effect of humidity can be neglected. Similarly, for a given value of force coefficient, the force varies linearly with density so humidity has little effect while temperature and pressure should be accounted for. This explains why the ball flies further in hot, high altitude venues since reduced air density reduces the drag force on the ball.

The impact of humidity beyond its effect on Re has been considered in a number of studies. Binnie [46] concluded that a condensation shock could upset a laminar boundary layer if the relative humidity is "*nearly 100%*". However, this mechanism would reduce the likelihood of conventional swing in humid conditions, as the critical Re for the non-seam side boundary layer would be reduced. Bentley et al. [28] and James [47] investigate the idea that the seam swells as it absorbs moisture from the air but their tests showed no measurable change in geometry due to humidity. Furthermore, changes to seam geometry are unlikely to effect the non-seam side flow which is the dominant factor in determining whether conventional swing can occur. Moore and Needes [8] measured no difference in swing force, at fixed Re, on days with different specific humidity levels between 20% and 50%, and Sherwin and Sproston [48] found no effect on the magnitude of swing with humidity varying between 61% and 100%. More recent tests by Scobie et al. [21] tested a new ball at 31%, 51% and 73% relative humidity and showed that there was "*no significant effect*" on C_S or Re at which the ball switches from conventional to reverse swing.

Finally, Steadman [49] studied differences in perceived temperature due to changes in humidity and wind speed. An increase in wind speed of 4m/s was found to have a similar effect on perceived temperature as a drop of 20-30% in humidity. This effect shows that days which are felt to be humid are also likely to have low wind speeds. The effect of wind on cricket ball swing is a transient condition and is considered in the next subsection.

Transient Conditions. Atmospheric conditions which vary from one delivery to the next, or during each delivery, are considered to be 'transient'. They are quantified with variables associated with the air flow across the pitch: wind speed, wind direction, and atmospheric turbulence, and need to be measured locally and time accurately.

The effect of wind speed on a cricket ball trajectory is included in the trajectory equations developed by Baker [20]. These show that for a ball travelling 18m released at 33.5m/s (75mph, Re=1.64×10^5), the inclusion of a 4m/s perpendicular crosswind in the model changes the lateral displacement by approximately 0.18m. This is 19% of the total lateral displacement for a swing force coefficient of 0.3 in such a crosswind. Baker's analysis assumes that the drag and swing force coefficients are defined as a function of Re only. However, a crosswind also changes the incidence of the oncoming air to the ball. This has the same effect as changing seam angle and with a ball speed of 33.5m/s and a perpendicular crosswind of 4m/s the angle change is 6.8°. As discussed in the previous section, C_S is sensitive to seam angle and a case where the wind changes the effective seam angle from positive to negative would change the direction and magnitude of the swing force. This effect is likely to be more important than that captured by Baker's existing model and should be included in future cricket ball trajectory modelling.

The principles of free-stream turbulence are presented by Taylor [50, 51, 52] as a statistical model to describe fluctuations in a flow where the time accurate flow field is split into its mean and fluctuating components as shown in Equation 7. The Turbulence Intensity is then defined in Equation 8 as the ratio of the root mean square of the fluctuation to the mean value.

$$U(t) = \overline{U} + U' \tag{7}$$

$$TI = \frac{(U')_{RMS}}{\overline{U}} \tag{8}$$

Papers on cricket ball swing by Baker [20], James [47] and Scobie et al. [21] hypothesise that freestream turbulence is generated from turbulent convection from a hot cricket pitch. This is linked to the belief that swing is less likely to occur on clear, sunny days. Scobie et al. cite work by Ibbetson [54] where meteorological measurements show velocity fluctuations up to 0.75m/s which equate to 4% turbulence intensity for a ball delivered at 38m/s (85mph). The discussion in the paper by Scobie et al. attributes the fluctuations to "*convective micro-turbulence*", though in the paper itself, Ibbetson says this is due to thermal convection *and* spatial variations of the wind velocity, without separating these effects out.

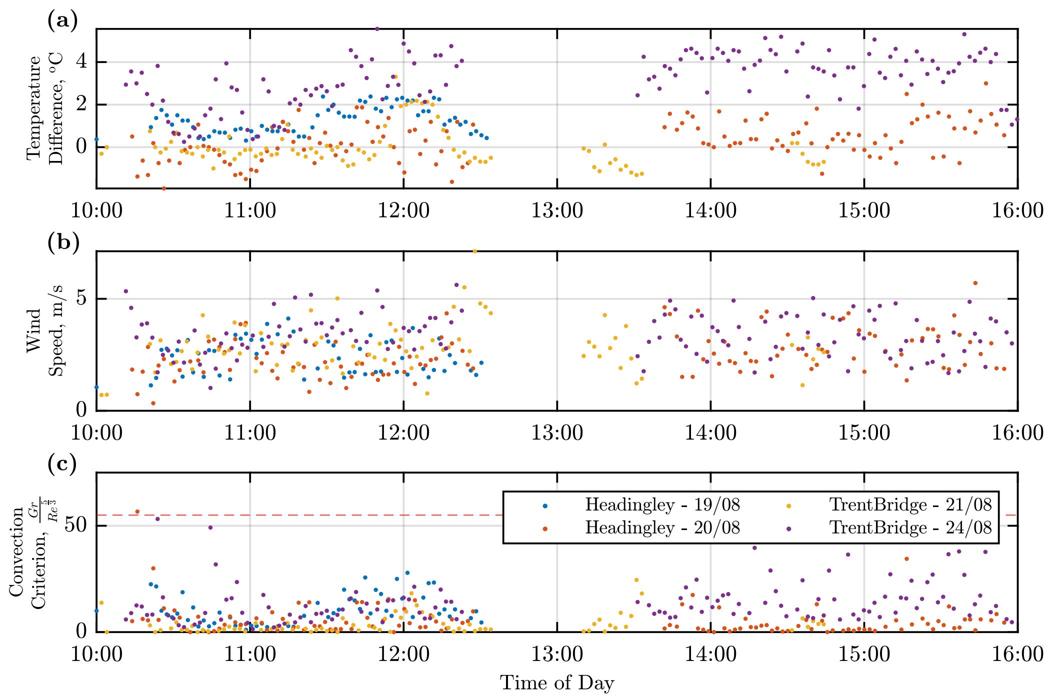

Figure 21. *Plots of (a) ground to air temperature difference, (b) wind speed and (c) convection criterion [53] measured on four separate days at two professional cricket venues in England.*

Wang [53] investigated buoyancy flows generated by a hot plate in a cross-flow which is analogous to a hot cricket pitch with wind blowing across it. Turbulent fluctuations are produced over the heated metal plate when free convection, driven by a temperature difference between the plate and the air, dominates the effect of flow across the plate. This effect is characterised by the ratio of the Grashof Number, Gr_x, to the Reynolds number of the flow across the plate, Re_x, and Wang's experiments show that convection driven turbulence occurs when:

$$\frac{Gr_{\mathrm{x}}}{(Re_{\mathrm{x}})^{\frac{5}{3}}} > 55.3 \tag{9}$$

For example, with a wind speed of 5m/s, the condition in Eq. 9 is met when ground temperature is 50°C greater than the air temperature. To test whether this condition is likely to occur in a cricket match, measurements of air and ground temperature and wind speed were taken at two professional cricket venues in England in the summer of 2020. Details of this test are included in Appendix A. Figure 21 shows that the critical value for the convection criterion from Wang's analysis was only exceeded once during the four days tested, with a maximum value of 56 and an overall mean of 14.9. The temperature difference between the ground and air is therefore not expected to drive freestream turbulence on the 'unremarkable' English summer days that the data was collected. Further work is required to establish whether ground to air temperature differences in hot countries, such as India or Australia, are large enough to drive freestream turbulence when the wind speed is low.

Figure 22 shows wind tunnel measurements reported by Scobie et al. [21] in which a new ball, labelled (A), is tested with a turbulence grid which generates free stream turbulence intensity of approximately 5%. C_S recorded is between -0.10 and -0.05 so conventional swing does not occur for $Re > 1.1 \times 10^5$. The same ball, tested with a turbulence intensity of approximately 1% when no turbulence grid is used, is labelled (B) in Fig. 6 and has C_S between 0.28 and 0.30 up to $Re = 2.1 \times 10^5$. The difference in behaviour

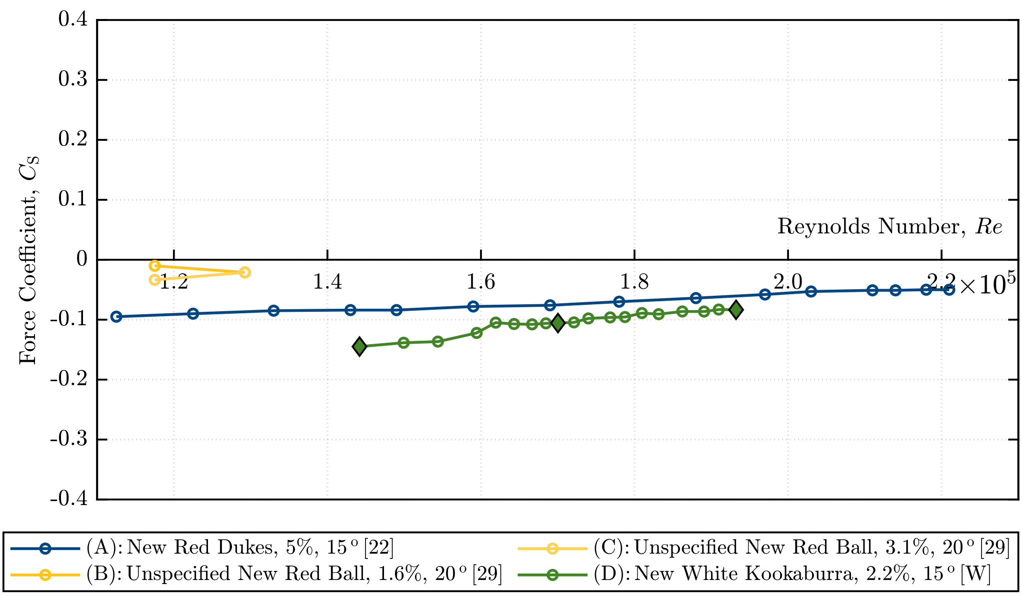

Figure 22. *Swing force coefficient, C_S plotted against Reynolds Number, Re, for wind tunnel experiments using grids to increase freestream turbulence intensity. The percentage value given in the legend is the recorded turbulence intensity of each test. IR images of the non-seam side are presented in Fig. 23 for the three cases highlighted with solid, diamond-shaped markers.*

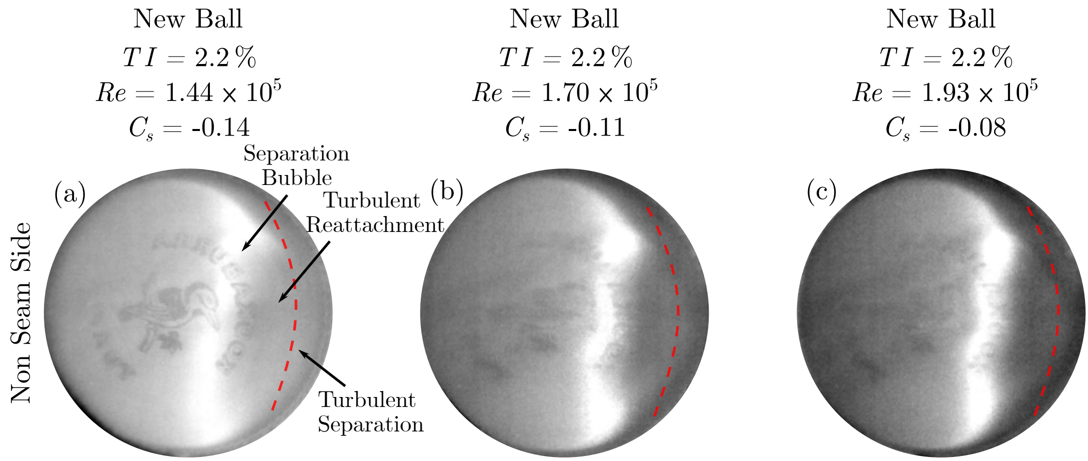

Figure 23. *Non-seam side IR image of a new cricket ball with grid-generated turbulent intensity of 2.2% for varying Re. Flow is left to right and red dashed lines illustrate eventual separation position.*

with and without the turbulence grid is because the increased turbulence reduces the critical Re for the non-seam side transition. This results in a laminar separation bubble and reattachment on the non-seam side at reduced Re and limits the flow asymmetry so that small negative C_S are recorded. Similar results were recorded for $Re < 1.3 \times 10^5$ by Bentley et al. [28] using the projection test approach and turbulence grids which gave turbulence intensities of 1.6% and 3.1%. This data is non-dimensionalised and reproduced in Fig. 22, labelled (B) and (C).

To validate Scobie et al.'s results, a turbulence grid which generates 2.2% turbulence intensity was added to the Whittle Laboratory test section and force and IR measurements recorded. The data, labelled (D) in Fig. 22, shows C_S between -0.15 and -0.09 for $Re = 1.44 - 1.93 \times 10^5$ and the same qualitative trend as Scobie et al.'s measurements. The IR images in Fig. 23 confirm that the non-seam side is above the critical value at $Re = 1.38 \times 10^5$ and has a laminar separation bubble and reattachment. Overall, freestream turbulence prevents conventional swing for $Re > 1.2 \times 10^5$ and the flow past the ball is best represented by the sketch in Fig. 17(a).

Studies using turbulence grids show that freestream turbulence intensity could be an important factor in determining whether a ball will swing. However, there is no published work on the range of turbulence intensities and length scales a cricket ball is likely to encounter, no study of how this turbulence is generated, and no systematic investigation of how turbulence intensity and length scale affect the non-seam side critical Re. All of these topics should be the subject of future work.

5.3. Summary

This section reviews and reassesses papers which consider 'Realistic Boundary Conditions' and these have been split into two topics, the effect of ball rotation and atmospheric conditions.

Experiments using a spinning mount in a wind tunnel are limited because interference between the mount and the flow, at a crucial position on the ball, cannot be avoided. Some of these limitations are overcome by projection tests, where swing is quantified by measuring the deflection of a spinning cricket ball as it falls through a wind tunnel jet. These experiments are less repeatable than fixed tests, however, through repeated measurement and averaging, Barton [35] and Bentley et al. [28] show that the switch from conventional to reverse swing happens over a Reynolds number range of approximately 0.4×10^5 with C_S varying smoothly in this range from 0.3 to -0.1. This more gradual change, compared to fixed wind tunnel tests shown in Fig. 6, is a better match to the ball tracking data shown in Fig. 2. We hypothesize that this is because a spinning ball can periodically switch the non-seam side between the sub and super critical regime by changing the seam angle from positive to negative through 'wobble' or by bringing features on the non-seam side towards the front of the ball. This averages the force experienced by the ball allowing C_S between 0 and 0.2 to be achieved.

Projection tests allow spin rate to be studied and both Bentley et al. and Barton conclude that there is an optimum spin rate for swing. However, the explanations given for this behaviour are not clear and further work is required to confirm the result and to determine the physical mechanisms involved. Spinning cricket balls have also been simulated using CFD. However, the results presented are not consistent with the experiments reviewed in the rest of this paper and no conclusions can be drawn about the effect of spin rate. Accurate CFD simulation of cricket ball swing has yet to be achieved and this represents an important area for future work.

Atmospheric conditions are split into macroscopic and transients effects. Variation in pressure, temperature and humidity are considered macroscopic because they vary slowly, on the order of hours, and effect an entire cricket ground. Changes in pressure and temperature change the Reynolds number of a delivery for a fixed ball speed and diameter via air density and viscosity, however, changes in humidity have a negligible effect, less than 1%, on Re. Previous studies in which humidity has been measured have not shown any effect.

The effect of wind speed, wind direction and freestream turbulence are considered transient conditions because they vary on a timescale of a delivery, or shorter, and have a local affect on the air which the ball is passing through. Wind changes the velocity of the flow approaching the ball in the ball frame of reference. This has three effects if there is a crosswind component: it changes Re, it moves the stagnation pressure point on the ball which has the same effect as changing the seam angle, and it varies the swing and drag force vectors in the absolute frame. The introduction of turbulence grids into wind tunnel experiments has shown that freestream turbulence prevents conventional swing with a new ball at $Re > 1.1 \times 10^5$. Further work is required to establish whether atmospheric turbulence is able to produce sufficient turbulence intensity, at suitable length scales in the ball frame of reference, to cause similar behaviour in match conditions.

Finally, it is noted that real boundary conditions are best represented as statistical distributions. A statistical model is required to represent variations in seam angle and ball orientation during each delivery due to spin, wind speed and direction, turbulence intensity, as well as differences between Re, average seam angle and ball condition from one delivery to the next. This will enable the distribution of swing coefficients observed in real match data to be understood and even predicted.

6. Conclusions and Recommendations

Research into cricket ball swing has been conducted for almost 70 years and while progress has been made through experimental study, the impact of scientific research on the game has been limited. Personal experience and anecdote still drive players, coaches, pundits and fans' understanding of swing and the tactical approach to swing bowling. This paper provides a review of the scientific literature and presents new experimental results which add to the work of others.

Conclusions are split in two, with the first set explaining how the boundary layer aerodynamics of the ball cause swing:

- Asymmetric boundary layer flow separation on each side of the ball causes a force which results in swing: Conventional swing occurs when the flow separates further back on the seam side of the ball than the non-seam side. Reverse swing occurs when the flow asymmetry is switched and the flow separates further back on the non-seam side than the seam side.
- For conventional swing, the non-seam side boundary layer remains laminar, separating approximately 80° from the stagnation point at the front of the ball when Re is below a critical value. On the seam side, streamwise coherent structures are shed from the seam and interact with the free shear layer downstream of a laminar separation, leading to a turbulent reattachment of the boundary layer which then separates at approximately 120°.

- Reverse swing with a new ball occurs when Re is high enough to cause transition on the non-seam side. The seam side flow is similar to the conventional swing case so overall asymmetry is reduced and the magnitude of C_S is 3 to 4 times smaller than for conventional swing.
- To maximise reverse swing, the seam side should be roughened while keeping the non-seam side smooth. This causes the laminar separation bubble on the seam side to close and the turbulent separation to move forwards. Asymmetry is increased, leading to C_S similar in magnitude to conventional swing.
- When both sides of the ball become rough, the non-seam side separation also moves forwards, meaning that there is less flow asymmetry and reverse swing is reduced.

The second set of conclusions relate to realistic boundary conditions encountered in cricket matches:

- Projection tests with spinning cricket balls show a switch from conventional to reverse swing over a Reynolds number range of approximately 0.4×10^5, with C_S varying smoothly in this range from 0.3 to -0.1.
- Changes in pressure and temperature affect Re for a fixed ball speed and diameter via air density and viscosity. Changes in humidity, however, have a negligible effect of less than 1% on Re and previous studies into humidity have not shown any effect on cricket ball swing.
- Wind across a cricket pitch changes Re, moves the stagnation pressure point on the ball if there is a crosswind component, and varies the swing and drag force vectors in the reference frame of the pitch.
- The introduction of turbulence grids into wind tunnel experiments has shown that freestream turbulence prevents conventional swing with a new ball for $Re > 1.1 \times 10^5$.

This paper also identifies areas requiring further study and these are gathered together as recommendations for future work:

- For static wind tunnel tests, balls should be tested at a range of Re and at varying seam, θ, and rotation angles, α. The results can then be averaged in a model for spinning and/or wobble seam balls to examine the discrepancy with ball tracking data.
- Future work should include testing on a large set of balls (> 20) so that statistical data can be gathered on the range and effect of defects.
- An optimum spin rate for swing, observed in projection tests in the 1980s, is not understood, so future work could reproduce the experiments, confirm the results and study the effect in more detail.
- A quantified relationship between surface roughness, k/D, Reynolds number, Re, and separation angle, ϕ_s, should be measured to enable the magnitude of reverse swing to be quantitatively linked to ball condition.
- Further work is required to establish whether atmospheric conditions at cricket grounds are able to produce turbulence which effects cricket ball swing as seen using turbulence grids in wind tunnels.
- Accurate CFD simulations of cricket ball swing have yet to be achieved. Modelling realistic boundary conditions, including surface roughness, and overcoming the limitations of turbulence modelling, make this a challenging and important area for future work.

By combining previous literature and results from new experiments, this paper establishes a deterministic understanding of cricket ball swing which is summarised for conventional swing in Fig. 13 and reverse swing in Fig. 17. However, the effect of key boundary conditions, including ball surface condition, ball orientation, wobble and spin, and atmospheric turbulence, have not yet been studied in detail or quantified. Doing this will require a statistical approach and it is expected that this will lead to scientific measurements and analyses which match more closely with match data and player experience.

Acknowledgements. We gratefully acknowledge the support of the England and Wales Cricket Board (ECB) and in particular our collaboration with Prof. Stafford Murray, Nathan Leamon and Dr Raph Brandon. We would also like to thank students and staff at the Whittle Laboratory for their interest in the project and in particular Prof. Graham Pullan and Prof. Tony Purnell for their input and guidance throughout the work, and Dr Chris Clark and Will Davis for their helpful comments on the draft manuscript. Finally, we are very grateful to the skilled technicians at the Whittle Laboratory for helping to set up the experiments and in particular Ian Thornton for constructing the wind tunnel working section.

Funding Statement. Dr Aaron Briggs gratefully acknowledges the funding of his PhD studies by the England and Wales Cricket Board (ECB). The authors would also like to thank Girton College, Cambridge and Kings College, Cambridge for their help in purchasing some of the experimental equipment used during the course of this work.

Competing Interests. The authors declare none.

Author Contributions. All three authors planned the study and worked closely together throughout the project. S.D.G. refined the literature review, wrote the manuscript and reproduced figures from other papers. A.B. produced the first literature review, completed the experimental campaign and produced figures of the new experimental results.

Data Availability Statement. The data in Figs 6, 7 and 22 are available in .csv format to download at https://whittle.digital/2024/Cricket_Ball_Swing. The IR images in Figs 12, 16 and 23 are also available unlabelled in .pdf and .svg format at the same link.

Ethical Standards. The research meets all ethical guidelines, including adherence to the legal requirements of the study country.

References

[1] International Cricket Council. *First global market research project unveils more than one billion cricket fans*. Available at https://www.icc-cricket.com/media-releases/759733. 2018.

[2] M. S. Taliep et al. "Event-Related Potentials, Reaction Time, and Response Selection of Skilled and Less-Skilled Cricket Batsmen". In: *Perception* 37.1 (2008). PMID: 18399250, pp. 96–105. DOI: 10.1068/p5620. eprint: https://doi.org/10.1068/p5620.

[3] N. Leamon and B. Jones. *Hitting Against the Spin: How Cricket Really Works*. eng. 2020. ISBN: 9781472131256.

[4] J.C. Cooke. "The Boundary Layer and "Seam" Bowling". In: *The Mathematical Gazette* 39.329 (1955), pp. 196–199. DOI: 10.2307/3608746.

[5] R. A. Lyttleton. "On the Swerve of a Cricket ball". In: *Weather* 12.5 (May 1957), pp. 140–146. ISSN: 14778696. DOI: 10.1002/j.1477-8696.1957.tb00464.x.

[6] J.W. Harrington and H. Southworth. "Asymmetrical Boundary Layers on Cylinders". MA thesis. Massachusetts Institute of Technology, 1957.

[7] J.D. Burgess and D. R. Probert. *An Investigation into the Flow Characteristics and Swing of a Cricket Ball*. Tech. rep. University of Cambridge, 1972.

[8] J. W. Moore and J. C. Needes. *The Effect of Humidity on the Swing of a Cricket Ball*. Tech. rep. University of Cambridge, 1973.

[9] J.H. Horlock. "The Swing of a Cricket Ball". In: *Proceedings of the ASME Symposium on Mechanics of Sport* 4 (1973).

[10] R. D. Mehta. "Aerodynamics of Sports Balls". In: *Annual Review of Fluid Mechanics* 17.1 (Jan. 1985), pp. 151–189. ISSN: 00664189. DOI: 10.1146/annurev.fluid.17.1.151.

[11] R. D. Mehta. "An Overview of Cricket Ball Swing". In: *Sports Engineering* 8.4 (Dec. 2005), pp. 181–192. ISSN: 1369-7072. DOI: 10.1007/bf02844161.

[12] R. D. Mehta. "Fluid Mechanics of Cricket Ball Swing". In: *19th Australasian Fluid Mechanics Conference*. 2014.

[13] S. Verma. "A Review on the Swing of a Cricket Ball". In: *IJSR-INTERNATIONAL JOURNAL OF SCIENTIFIC RESEARCH* 4 (), pp. 420–424.

[14] J. A. Scobie et al. "Fluid Dynamics of Cricket Ball Swing". In: *Proceedings of the Institution of Mechanical Engineers, Part P: Journal of Sports Engineering and Technology* 227.3 (2013), pp. 196–208. ISSN: 17543371. DOI: 10.1177/1754337112462320.

[15] R. W. Jackson et al. "Investigation of Reverse Swing and Magnus Effect on a Cricket Ball using Particle Image Velocimetry". In: *Applied Sciences (Switzerland)* 10.22 (2020), pp. 1–15. ISSN: 20763417. DOI: 10.3390/app10227990.

[16] J. Tom et al. "CFD Analysis of Swing of Cricket Ball and Trajectory Prediction". In: *APS Division of Fluid Dynamics Meeting Abstracts*. 2013, H5–006.

[17] N. Owens and A. Dixon. "Intelligent Visual Analysis for Sports Production". In: *1st European Conference on Visual Media Production (CVMP) 2004*. 2004, pp. 31–38.

[18] H. Schlichting. *Boundary Layer Theory*. eng. Ninth edition. 2016. ISBN: 9783662529195.

[19] Z. Yang. "On Bypass Transition in Separation Bubbles: A Review". In: *Propulsion and Power Research* 8.1 (2019), pp. 23–34.

[20] C. J. Baker. “A Calculation of Cricket Ball Trajectories”. In: *Proceedings of the Institution of Mechanical Engineers, Part C: Journal of Mechanical Engineering Science* 224.9 (Sept. 2010), pp. 1947–1958. ISSN: 09544062. DOI: 10.1243/09544062JMES1973.

[21] J. A. Scobie et al. “Practical Perspective of Cricket Ball Swing”. In: *Proceedings of the Institution of Mechanical Engineers, Part P: Journal of Sports Engineering and Technology* 234.1 (2020), pp. 59–71. ISSN: 1754338X. DOI: 10.1177/1754337119872874.

[22] R. Deshpande, R. Shakya, and S. Mittal. “The Role of the Seam in the Swing of a Cricket Ball”. In: *Journal of Fluid Mechanics* 851 (2018), pp. 50–82. ISSN: 14697645. DOI: 10.1017/jfm.2018.474.

[23] A. T. Sayers and A. Hill. “Aerodynamics of a Cricket Ball”. In: *Journal of Wind Engineering and Industrial Aerodynamics* 79.1-2 (Jan. 1999), pp. 169–182. ISSN: 01676105. DOI: 10.1016/S0167-6105(97)00299-7.

[24] F. Alam et al. “Aerodynamics of Used Cricket Balls”. In: *17th Australasian Fluid Mechanics Conference 2010*. 2010. ISBN: 9781617829130.

[25] L. Tadrist et al. “When can you expect contrast swing in a cricket game, and how to obtain it?” In: *Sports Engineering* 23 (2020), pp. 1–10.

[26] E. Achenbach. “Experiments on the Flow Past Spheres at Very High Reynolds Numbers”. In: *Journal of Fluid Mechanics* 54.3 (Aug. 1972), pp. 565–575. ISSN: 14697645. DOI: 10.1017/S0022112072000874.

[27] E. Achenbach. “The Effects of Surface Roughness and Tunnel Blockage on the Flow Past Spheres”. In: *Journal of Fluid Mechanics* 65.1 (Aug. 1974), pp. 113–125. ISSN: 14697645. DOI: 10.1017/S0022112074001285.

[28] K. Bentley. “An Experimental Study of Cricket Ball Swing”. In: *Imperial College Aero Technical Note* (1982), pp. 82–106.

[29] A. T. Sayers. “On the Reverse Swing of a Cricket Ball - Modelling and Measurements”. In: *Proceedings of the Institution of Mechanical Engineers, Part C: Journal of Mechanical Engineering Science* 215.1 (Jan. 2001), pp. 45–55. ISSN: 09544062. DOI: 10.1243/0954406011520508.

[30] K. Son et al. “Mechanism of Drag Reduction by a Surface Trip Wire on a Sphere”. In: *Journal of Fluid Mechanics* 672 (Apr. 2011), pp. 411–427. ISSN: 14697645. DOI: 10.1017/S0022112010006099.

[31] M. Gad-El-Hak and D.M. Bushnell. “Separation Control”. In: *Journal of fluids engineering* 113.1 (1991), pp. 5–30.

[32] P. N. Joubert and E. R. Hoffman. “Drag of a Circular Cylinder with Vortex Generators”. In: *The Journal of the Royal Aeronautical Society* 66.619 (July 1962), pp. 456–457. ISSN: 0368-3931. DOI: 10.1017/s0368393100076987.

[33] G. Schewe. “Sensitivity of Transition Phenomena to Small Perturbations in Flow Round a Circular Cylinder”. In: *Journal of Fluid Mechanics* 172.-1 (Nov. 1986), pp. 33–46. ISSN: 14697645. DOI: 10.1017/S0022112086001635.

[34] K. Shah and S. Mittal. “Is a Baseball like Knuckleball Possible in Cricket?” In: *Flow* 3.E16 (2023).

[35] N. G. Barton. “On the Swing of a Cricket Ball in Flight”. In: *Proceedings of the Royal Society of London* 379 (1982), pp. 109–131.

[36] S. Taneda. “Visual Observations of the Flow Past a Sphere at Reynolds Numbers between 10^4 and 10^6”. In: *Journal of Fluid Mechanics* 85.1 (Mar. 1978), pp. 187–192. ISSN: 14697645. DOI: 10.1017/S0022112078000580.

[37] R.D. Mehta and J.M. Pallis. “The Aerodynamics of a Tennis Ball”. In: *Sports Engineering* 4.4 (2001), pp. 177–189.

[38] F. Alam et al. “A Study of Baseball and Softball Aerodynamics”. In: *Procedia Engineering* 34 (2012), pp. 86–91.

[39] F. Alam et al. “A Comparative Study of Football Aerodynamics”. In: *Procedia Engineering* 2.2 (2010), pp. 2443–2448.

[40] P.W. Bearman and J.K. Harvey. “Golf Ball Aerodynamics”. In: *Aeronautical Quarterly* 27.2 (1976), pp. 112–122.

[41] R. Latchman and A. Pooransingh. “Modeling Conventional Swing of a Cricket Ball”. In: *Proceedings of the 2015 COMSOL Conference Boston. Retrieved*. Vol. 24. 2015.

[42] S. Kalburgi et al. “Computational Fluid Dynamics Study of Cricket Ball Aerodynamics Associated with Swing”. In: *Journal of Advanced Research in Fluid Mechanics and Thermal Sciences* 75.2 (2020), pp. 125–136. ISSN: 22897879. DOI: 10.37934/arfmts.75.2.125136.

[43] D.G. Pahinkar and J. Srinivasan. “Simulation of Reverse Swing of the Cricket Ball”. In: *International Journal of Sports Science and Engineering* 4.1 (2010), pp. 053–064.

[44] M. Johnson. “Ashes 2019: Without Jofra Archer, England’s Bowling Attack is Weaker than Australia’s”. In: *i News UK* (2019).

[45] P. T. Tsilingiris. “Thermophysical and Transport Properties of Humid Air at Temperature Range between 0 and 100 °C”. In: *Energy Conversion and Management* 49.5 (May 2008), pp. 1098–1110. ISSN: 01968904. DOI: 10.1016/j.enconman.2007.09.015.

[46] A. M. Binnie. “The Effect of Humidity on the ‘Swing’ of Cricket Balls”. In: *International Journal of Mechanical Sciences* 18.9-10 (1976), pp. 497–499. ISSN: 00207403. DOI: 10.1016/0020-7403(76)90046-1.

[47] D. James, D. C. MacDonald, and J. Hart. “The Effect of Atmospheric Conditions on the Swing of a Cricket Ball”. In: *Procedia Engineering*. Vol. 34. 2012, pp. 188–193. DOI: 10.1016/j.proeng.2012.04.033.

[48] K. Sherwin and L. Sproston. “Aerodynamics of a Cricket Ball”. In: *International Journal of Mechanics* 10.2 (1982), pp. 71–79.

[49] R. G. Steadman. “The Assessment of Sultriness. Part II: Effects of Wind, Extra Radiation and Barometric Pressure on Apparent Temperature”. In: *Journal of Applied Meteorology (1962-1982)* 18.7 (1979), pp. 874–885. ISSN: 00218952, 2163534X.

[50] G. I. Taylor. “Diffusion by Continuous Movements”. In: *Proceedings of the London Mathematical Society* s2-20.1 (Jan. 1922), pp. 196–212. ISSN: 1460244X. DOI: 10.1112/plms/s2-20.1.196.

[51] G. I. Taylor. "Statistical Theory of Turbulence". In: *Proceedings of the Royal Society of London. Series A - Mathematical and Physical Sciences* 151.873 (Sept. 1935), pp. 421–444. ISSN: 0080-4630. DOI: 10.1098/rspa.1935.0158.

[52] G. I. Taylor. "The Spectrum of Turbulence". In: *Proceedings of the Royal Society of London. Series A - Mathematical and Physical Sciences* 164.919 (Feb. 1938), pp. 476–490. ISSN: 0080-4630. DOI: 10.1098/rspa.1938.0032.

[53] X. A. Wang. "An Experimental Study of Mixed, Forced, and Free Convection Heat Transfer from a Horizontal Flat Plate to Air". In: *Journal of Heat Transfer* 104.1 (Feb. 1982), pp. 139–144. ISSN: 15288943. DOI: 10.1115/1.3245040.

[54] A. Ibbetson. "Topics in Dynamical Meteorology: Some Aspects of the Description of Atmospheric Turbulence". In: *Weather* 33.10 (1978), pp. 369–382. ISSN: 14778696. DOI: 10.1002/j.1477-8696.1978.tb04611.x.

[55] P. E. Roach. "The Generation of Nearly Isotropic Turbulence by Means of Grids". In: *International Journal of Heat and Fluid Flow* 8.2 (June 1987), pp. 82–92. ISSN: 0142727X. DOI: 10.1016/0142-727X(87)90001-4.

7. Appendix A: Experimental Methods

Experimental work was carried out using an open circuit, low speed wind tunnel, situated in the Whittle Laboratory at the University of Cambridge.

7.1. Wind tunnel test section

Figure 24 shows the test section of the wind tunnel which has dimensions of 450 mm ×450 mm ×1000 mm ($W \times H \times L$). The wind tunnel is capable of delivering a maximum flow speed of U_{tunnel} = 43 m/s, equivalent to 96 mph, similar to the maximum speeds achieved by fast bowlers in professional cricket.

The stagnation pressure and static pressure at inlet to the test section are measured by a Scanivalve DSA3217 Pressure Scanner connected to Pitot and static pressure probes. A thermocouple is mounted next to the pressure probes, and the atmospheric pressure and humidity are recorded remotely via a Vaisala PTU300 pressure, temperature and humidity (PTH) sensor mounted in the laboratory. These measurements are used to evaluate the flow speed, air density and air viscosity and these are used to calculate the Reynolds number of the flow.

The turbulence intensity level in the tunnel is changed using a horizontal bar turbulence grid upstream of the test section. A one-dimensional, straight hot-wire probe is connected to a Dantec hotwire holder and a Dantec StreamLine Pro Constant Temperature Anemometer (CTA) is used to generate voltage signals from the probe. These voltages are recorded using a National Instruments USB-4431 voltage input module at a rate of 50 kHz. The turbulence grid is designed using equations from Roach[55] to ensure appropriate turbulence intensity and length scales in the working section, and has a blockage ratio less than 5%. Different turbulence levels are achieved by varying the bar thickness, which can be interchanged using 3D printed mounts at the side of the tunnel.

7.2. Cricket Balls

Results for four types of cricket ball tested at the Whittle Laboratory are presented in this paper:

- New red, Test Match grade Dukes
- New white, One Day International grade Kookaburra
- Artificially roughened red, Test Match grade Dukes
- Artificially roughened red, Test Match grade Kookaburra

Roughness is generated with a sand-blaster which uses compressed air to propel sand at the ball, causing abrasion to the surface. The primary seam is masked during the process so is not degraded. Sand-blasting provides a more uniform roughness than other forms of artificial degradation, such as sand paper, and is found to be a more repeatable process. The roughness generated by the sand-blasting is measured with a Taylor Hobson Surtronic S-128 portable surface roughness tester with has a resolution of 10nm.

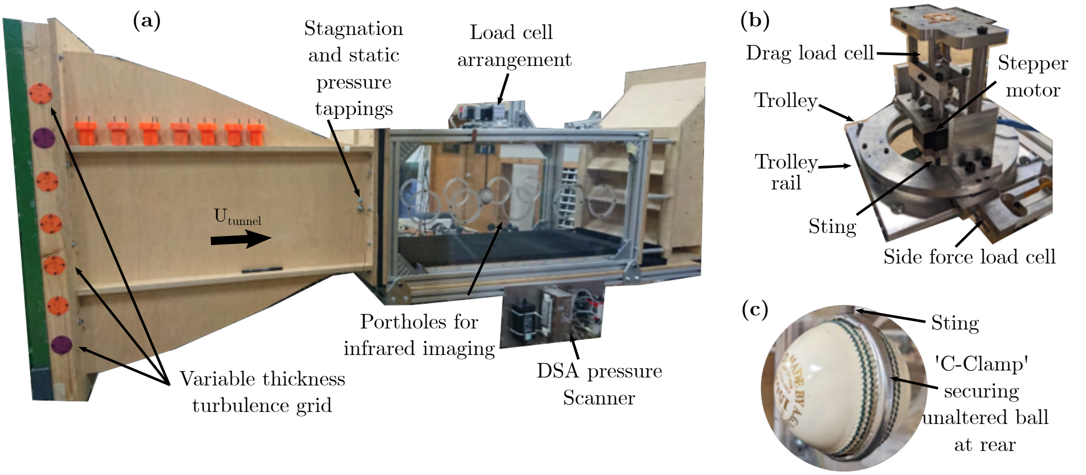

Figure 24. *Experimental configuration for testing real cricket balls in the wind tunnel. (a) Wind tunnel test section. (b) Labelled load cell arrangement for measuring forces on a ball. (c) C-clamp used to secure balls, which runs around the back of the seam.*

7.3. Ball mount

Cricket balls are mounted on a sting from the top of the test section, via a clasp called a ‘C-clamp’. The C-clamp, shown in Fig. 24(c) runs around the seam at the back of the ball with respect to the airflow. The ball is held securely using the tension in the curved shape meaning that unaltered cricket balls can be mounted and dismounted in seconds. The sting at the top of the clamp is mounted on a rotary table which controls the seam angle with respect to the flow, via a stepper motor as shown in Fig. 24(b). An aerodynamic fairing is placed around the sting, but not in contact with it, to minimise parasitic drag.

7.4. Force measurement

Drag and swing forces on the cricket ball are measured with Huntleigh load cells and recorded via a National Instruments 9236 C-Series strain input module. To isolate the drag and side force, the mounting for the ball, including the rotary table, is placed on a low friction trolley, shown in Fig. 24(b). The load cells are calibrated using known masses, and recorded at a frequency of 20kHz to monitor unsteady forces. The forces presented in this study are time averaged measurements taken over a 10s time period.

7.5. Infra red boundary layer visualisation

Boundary layer flow visualisation is performed at the same time as the force measurements using FLIR A615 infra red cameras. A temperature difference between the ball and the wind tunnel flow is established by chilling the balls in a refrigerator to approximately 5°C. The images captured are black and white, and provide a qualitative measure of the surface temperature, and hence the boundary layer flow, of the ball being tested.

7.6. Field test weather measurements

For outdoor field measurements, two pieces of bespoke hardware were designed, tested and manufactured: a datalogger, to record macroscopic atmospheric conditions, and a pneumatic wind sensor to measure mean wind speed and direction. The battery-powered equipment was able to record for approximately 8 hours without recharging, to track the changing conditions throughout a given day.

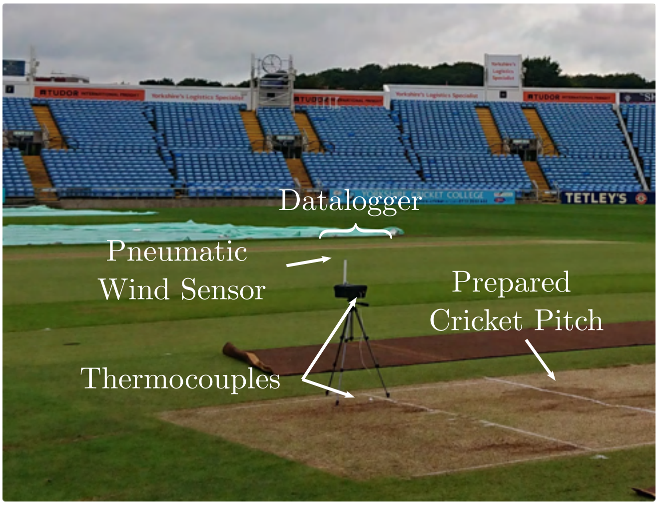

Figure 25. *Example set-up for measuring atmospheric conditions, shown here at Leeds Headingley cricket ground.*

The datalogger consists of an ADAFRUIT FEATHER M0 ADALOGGER micro-controller board, which records air and ground thermocouples, each connected to a MCP9600 thermocouple sensor, a BME680 environmental sensor for pressure and humidity and a VEML7700 light sensor. The sensors are packaged in a shockproof plastic case, mounted on a tripod, shown in Fig. 25.

The pneumatic probe used to measure wind speed and direction is constructed from six sealed hypodermic tubes of diameter 1.1mm, arranged in a hexagonal pattern inside a larger stainless steel tube of outer diameter 6.0mm. Holes are drilled normal to the probe surface, through the outer tube and into the six inner tubes, to create six evenly spaced pressure tappings around the circumference of the probe. Each inner tube is connected to a Honeywell pressure sensor with a range of ±250 Pa, suitable for measuring the small pressures generated by low wind speeds. The probe is mounted through the top of the datalogger case. A motorised sheath is fitted around the entire pneumatic sensor, and this is raised from the case to shield the tappings from the wind during zero offset calibrations.

To calibrate for wind speed and angle, the probe is mounted in a wind tunnel where reference velocities and flow angles are known. The probe is rotated through 360° and the six pressure tapping measurements recorded. For a given flow angle, one tapping will have the highest pressure and this is modelled as a centre hole in a three-hole probe arrangement. Non-dimensional yaw, stagnation pressure and static pressure coefficients are formed and six sets of overlapping calibration maps are generated for the 360° revolution. The calibration is repeated at three freestream velocities from 1.6m/s to 10.8m/s. Test results recorded in the field are non-dimensionalised and the calibration maps interpolated to 'look up' the flow angle, stagnation pressure and static pressure so the wind direction and speed can be calculated.

Cite this article: Grimshaw, S. D., Briggs, A. A., & Atkins, N. R. (2023). A Review and Reassessment of the Aerodynamics of Cricket Ball Swing. *Flow*, *1*, E1. doi:10.1017/flo.2023.1